

A new methodology to calculate process rates in a KMC model of PAH growth

Gustavo Leon¹, Nick Eaves², Jethro Akroyd^{1,3}, Sebastian Mosbach^{1,3},
Markus Kraft^{1,3,4}

released: March 20, 2019

¹ Department of Chemical Engineering
and Biotechnology
University of Cambridge
Philippa Fawcett Drive
Cambridge, CB3 0AS
United Kingdom

E-mail: mk306@cam.ac.uk

² Department of Mechanical, Automotive
and Materials Engineering
401 Sunset Avenue
Windsor, ON
Canada
N9B 394

³ CARES
Cambridge Centre for Advanced
Research and Education in Singapore
1 Create Way
CREATE Tower, #05-05
Singapore, 138602

⁴ School of Chemical
and Biomedical Engineering
Nanyang Technological University
62 Nanyang Drive
Singapore, 637459

Preprint No. 224



Edited by

Computational Modelling Group
Department of Chemical Engineering and Biotechnology
University of Cambridge
Philippa Fawcett Drive
Cambridge CB3 0AS
United Kingdom

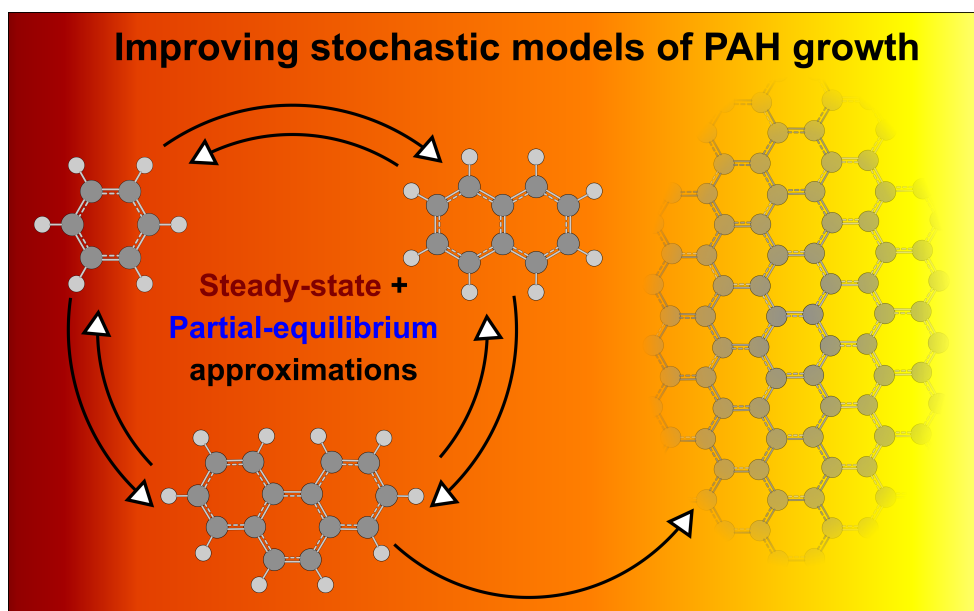
E-Mail: c4e@cam.ac.uk

World Wide Web: <http://como.ceb.cam.ac.uk/>



Abstract

This paper develops a new methodology to calculate the process rates in a kinetic Monte Carlo (KMC) model of polycyclic aromatic hydrocarbon (PAH) growth. The methodology uses a combination of the steady-state and partial-equilibrium approximations. It shows good agreement with the results from simulations using a detailed chemical mechanism under conditions relevant to flames (temperatures between 1000 and 2500 K, equivalence ratios between 0.5 and 10). The new methodology is used to calculate the rate of different stochastic processes in KMC simulations of PAH growth of premixed ethylene-oxygen flames. The resulting rates are only a function of temperature and the main gas-phase species present in the flame environment. The results of the KMC model are shown to be consistent with the concentrations of species calculated using a well-established mechanism for the growth of small PAH species.



Highlights

- Development of a combined steady-state and partial-equilibrium approximation.
- Stochastic jump process rate calculation consistent with the chemistry of small gas-phase PAHs.
- Applied in KMC model of PAH formation in premixed flame.

Contents

1	Introduction	3
2	Timescale separation approximations in models of PAH growth	4
3	Methodology	7
4	Results and discussion	8
4.1	Steady-state approximation	8
4.2	Partial-equilibrium approximation	11
4.3	A combined steady-state–partial-equilibrium approximation	13
4.4	A combined steady-state–partial-equilibrium KMC model	15
5	Conclusions	19
A	Appendices	20
A.1	Steady-state and partial-equilibrium model equations	20
A.1.1	General reaction equations	20
A.1.2	Production and loss terms	20
A.1.3	Approximations based on timescale separation	21
	Steady-state approximation	21
	Partial-equilibrium approximation	23
A.2	Steady-state and partial-equilibrium reactions and species	24
A.2.1	Treatment of non-partial-equilibrium reactions	32
A.2.2	Calculation of KMC jump process rates	33
A.3	Effect of ring condensation reactions	33
	References	35

1 Introduction

Polycyclic aromatic hydrocarbons (PAHs) are produced during the combustion of hydrocarbon fuels. These molecules are typically stable under flame conditions [73] and negatively affect human health [42, 46]. PAHs play a crucial role in the formation of carbonaceous particles including soot, which has been shown to be toxic [36, 54] and has serious climate repercussions [48, 61].

Soot grows as a result of the interactions between PAHs, hydrocarbons and free radical species in flames. PAHs play a significant role in the growth of soot and are believed to participate in the inception process [80]. For this reason, significant research has been invested to develop an accurate understanding of PAH growth as part of a wider effort to understand how PAHs and soot form and grow in a combustion environment.

The hydrogen abstraction, acetylene addition (often referred to as HACA) mechanism is widely considered the main route to explain the growth of PAH species [21, 80]. The WF mechanism [81] and subsequently the ABF mechanism [2] were some of the first studies to describe the growth of small gas-phase PAHs by assuming successive HACA sequences. The mechanism has been widely used and shows good agreement with experimental measurements [2, 50, 64]. Reactions from the ABF mechanism have been included in a number of modern mechanisms, including the DLR mechanism [13, 69, 70], the KM2 mechanism [82, 83], the CRECK mechanism [62, 63] and the Caltech mechanism [5, 53]. These include improved small hydrocarbon chemistry and additional routes towards the production of small PAHs like the contribution of cyclopentadiene or indene. These works use HACA sequences to explain the growth of larger PAHs, similar to the ABF mechanism.

It is widely thought that soot particles are incepted from moderately sized PAHs, of the order of 10–16 rings [1, 6, 7, 51]. It is therefore desirable that simulations of PAH and soot growth are able to describe the evolution of such PAHs. It is very common for simulations of PAH growth leading to soot formation to use chemical mechanisms similar to those discussed above to describe the composition of the gas-phase. Typically these simulations solve an ordinary differential equation (ODE) for the concentration of each species. However, the number of possible PAH species far exceeds the number of ODEs that can be solved in practical simulations. For this reason, the PAH growth pathways in the chemical mechanisms must be truncated. For practical reasons the truncation occurs at PAH sizes much smaller than the sizes thought to be relevant to soot formation. For example, the mass of PAHs forming nascent soot particles has been shown to be larger than the mass of the largest PAHs contained in mechanisms [12, 33].

Rather than solving an ODE for the concentration of each species (mathematically this is known as a *particle number model* because the model solves for the number concentration of each entity, in this case each species), an alternative approach is to use a stochastic numerical method to simulate the evolution of each entity within a given control volume (mathematically this is known as a *particle model*). This approach is the basis of kinetic Monte Carlo (KMC) models [28] and is suitable for problems with a very large number of species. These schemes use a set of reaction rules to simulate the growth of an ensemble of molecules, where the rules are often expressed in terms of reactions occurring at different

sites with rates that are extrapolated from analogous gas-phase reactions.

A number of KMC models have been used to investigate in detail the growth of individual PAH molecules. This approach allows fundamental insight into the PAH chemistry and possible reaction pathways. Using this type of model Frenklach and co-workers studied the surface growth rate of single soot particles [20], the growth of graphene-like structures [84, 85], the evolution of graphene under oxidising conditions [67] and soot particle oxidation [26]. Violi and collaborators applied this type of model to investigate the growth of soot precursors [43, 79], soot nucleation [38] and the effect of oxygen addition on PAH growth [16, 18].

KMC models have also been used in the context of coupled simulations of PAH growth and soot formation. Although methods have been developed to couple such models to the gas-phase chemistry [9, 11], the prevailing methodology is to perform the simulation as a post-process, having first solved the gas-phase chemistry by some other means. This approach has been used to reproduce experimental laser ionisation mass spectra [12], particle size distributions [8, 10, 65] and study the coagulation efficiency of soot particles [59]. In these cases, the model must simulate the growth of a large ensemble of PAHs. In these models, a simpler KMC scheme is required in order to keep the computations tractable. One example of such a difficulty with PAH-KMC schemes is that they can spend high computational effort to simulate reversible reactions where the forward and reverse rates are large, but where there is only a small net rate of change. Often this type of problem can be solved by estimating the contributions of intermediate species using steady-state or partial-equilibrium approximations [for example 20, 58]. It is of course important to ensure consistency between the approximated system and the original mechanism.

The purpose of this work is to investigate the range of validity of the steady-state and partial-equilibrium approximations in the context of PAH-KMC models [12, 58, 86]. The paper presents a new methodology to compute the concentrations of PAH reaction intermediates based on a combination of both approximations and computes a modified rate equation. The methodology is formulated such that is consistent with the available gas-phase mechanisms and such that it is suitable for inclusion in future KMC models of PAH growth and soot formation.

2 Timescale separation approximations in models of PAH growth

Timescale separation approximations often allow a simplified numerical treatment of the processes that control a reaction system. They are based on the separation of *fast* and *slow* processes. Typically a subset of the species concentrations are able to be estimated by solving a linear system of equations (as opposed to coupled ODEs). Examples of such techniques are the steady-state and partial-equilibrium approximations that we study in this paper. Both methods are well-documented in the literature [29, 31, 44, 55, 75, 76]. The model equations are summarised in Section A.1 of the Appendix.

A number of related approximations have been used in other applications. For example,

the simulation of turbulent combustion [56] and the generation of skeletal mechanisms [57]. Methods worth mentioning are intrinsic lower dimensional manifolds [30, 47], computational singular perturbation [31, 32, 57] and rate-controlled constrained equilibrium [4, 39, 40]. The reader is referred to [29, 44, 55, 75] for a review of these techniques.

Timescale separation approximations can be applied to the reactions that control the growth of PAHs. The HACA mechanism describes the consecutive production of radicals and addition of acetylene molecules. Each intermediate step in the mechanism has a different kinetic behaviour that needs to be analysed to identify possible timescale separations. Figure 1 shows an example of the reaction routes that are available for the growth of the most basic PAH, benzene growing to form naphthalene.

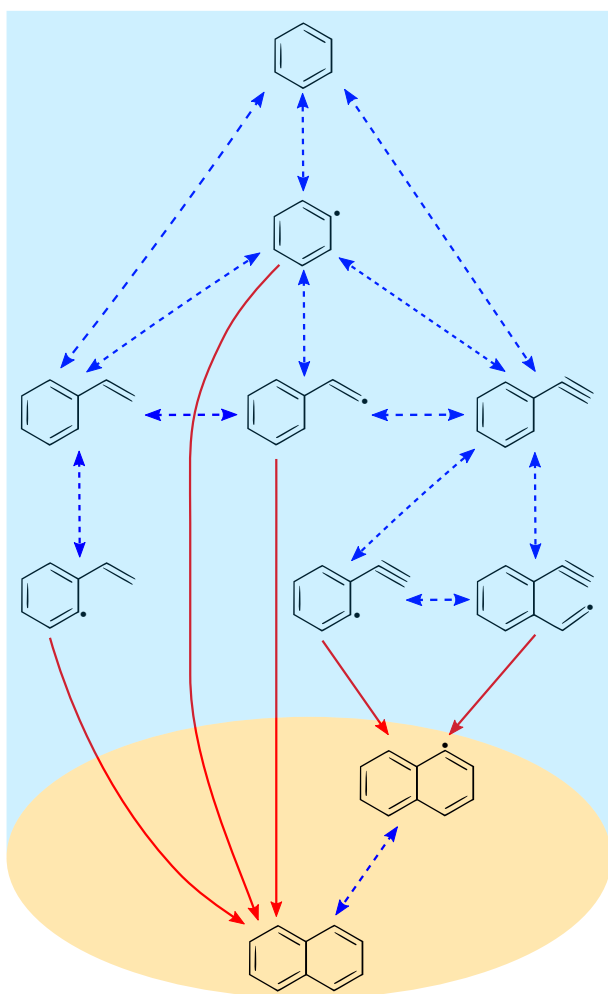


Figure 1: Reaction path flux diagram showing the main reaction pathways between benzene and naphthalene. Dashed blue arrows show reaction fluxes that are similar in magnitude in both directions. Continuous red arrows show reaction fluxes with reverse rates that are at least an order of magnitude smaller than the forward rate at early times under flame conditions.

In Figure 1 reactions are shown as arrows and for simplicity only a single arrow is shown when multiple reaction pathways are involved between two species. The figure not only

illustrates some of the main reaction pathways in PAH growth, it also shows the behaviour that can be observed for some of the intermediate species. Some reactions, shown as dashed blue arrows, are typically fast in both the forward and reverse ways, while others, shown as continuous red arrows, are usually fast only in one direction due to the high stabilisation that the formation of a new aromatic ring can provide. This behaviour allows a separation of fast and slow species that can be exploited to model the growth of this type of molecule.

The concentrations of fast-forming intermediates can often be estimated using a steady-state or partial-equilibrium approximation. In such cases, the concentration of these fast-forming intermediates can be calculated by solving a linear system of the form

$$Mc = b \tag{1}$$

where M is an $N_f \times N_f$ matrix and contains pseudo first-order rate constants for the consumption and production of each of the fast species, c is the vector of the N_f concentrations of the fast species, b is a vector that contains the production terms of fast species from slow species and N_f is the number of fast species. The model equations and assumptions behind them are summarised in Section A.1 of the Appendix.

The steady-state approximation has been widely used to analyse PAH chemistry. Early works on the HACA pathways used it to explore the high and low temperature limits of the mechanism [19, 21]. It has also been used to obtain single-step rates for addition reactions [52] and to estimate the concentration of intermediate PAHs that participate in soot inception [72]. Recently, the rate constants for the HACA pathways have been re-examined in different studies in which a steady-state approximation was applied with improved rate coefficients [27, 49], and which concluded that the HACA routes are the main growth pathways in most flame conditions.

The steady-state approximation has also been used to estimate the number of active sites on the surface of soot particles for a simple surface mechanism including five reactions [23]. This approach estimates the number density of the available carbon-hydrogen sites and requires the specification of an α -parameter (see [22] for a discussion of this parameter) as the fraction of sites that will be available to react. Such an approach has been used in multiple studies [17, 64] and has been modified to account for reversibility [15], additional pathways [83] and particle ageing effects [41, 66, 78]. Recently, an alternative approach that expresses the instantaneous value of α in terms of state variables based on consideration of the number of zig-zag and armchair sites has been proposed [22].

The steady-state approximation has been incorporated into a number of KMC models of PAH growth. The fast-lived intermediates that are formed in some HACA reactions have been modelled with this approach in the works of Frenklach and co-workers [20, 67, 68, 84, 85]. This allows the study of PAH growth without the need to spend long computational times simulating highly reversible reactions. KMC models that simulate an ensemble of PAHs have used this approximation to derive simplified rate equations for various reaction sequences [10, 12, 35, 58, 59, 86]. In these studies, the model describes a number of pathways for the addition and desorption of aromatic rings [58]. However, the model makes a number of simplifications including assuming irreversible acetylene addition and irreversible ring closures. A methodology that accounts for the reversibility of these steps and that is valid across a wide range of conditions is still required.

3 Methodology

In this work we study the range of validity of the steady-state and partial-equilibrium approximations of the chemical reactions that control the growth of gas-phase PAHs with the purpose to provide simplified rate equations for KMC models. In order to do so, we consider ethylene-air simulations in a closed control volume under isothermal and isobaric conditions at a pressure of one atmosphere. The effect of temperature and initial equivalence ratio was studied. The temperature was varied from 1000 to 2500 K in 100 K intervals. The equivalence ratios considered were 0.5, 1.0, 2.0, 5.0 and 10. All reaction systems were solved until a stationary solution was observed.

The ABF mechanism [2] was selected as a reference mechanism for this study for the following reasons: Its PAH reaction pathways contain mostly HACA sequences which, although they do not explain all the pathways for the production of some small PAHs, are able to explain the growth of larger molecules and are included in modern mechanisms [5, 60, 69]. It includes ring condensation reactions which have been shown to be important for PAH growth [77]. It includes five-member ring growth and armchair closure reactions, both of which are fast processes that have been shown to affect the shape of larger PAHs [10, 20]. Lastly, by choosing a mechanism that does not contain additional routes that are unique to small PAHs, for example the production of naphthalene from cyclopentadiene or indene, we can infer the rates of reaction for analogous processes acting on arbitrarily-sized PAHs. For example, by treating the growth rate of naphthalene from benzene (see Figure 2) as a proxy for a free-edge ring growth reaction.

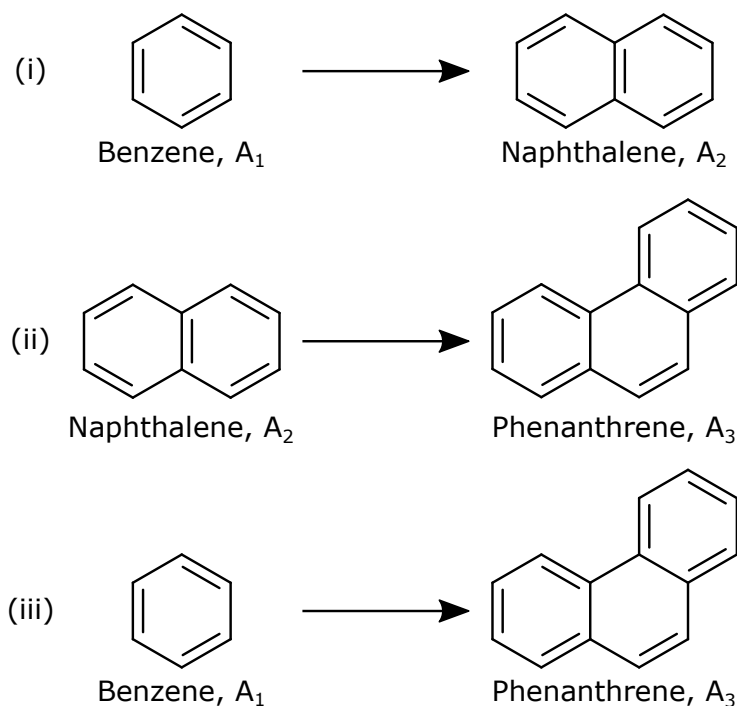


Figure 2: Ring growth processes studied using the steady-state and partial-equilibrium approximations. Notation as defined by Frenklach et al. [24].

New steady-state and partial equilibrium approximations are proposed to calculate the rates of the ring growth processes shown in Figure 2. Processes (i) and (ii) follow the HACA pathways starting from different PAHs. Process (iii) corresponds to ring condensation reactions where two benzene intermediates react to form phenanthrene. For each process, a linear system resulting from a steady-state or partial equilibrium approximation is solved for the concentration of key intermediate species. The resulting process rate is then a function of only the concentrations of main gas-phase species and the morphology of the PAH. This procedure can be generalised to obtain the process rates for any arbitrarily-sized PAH in a KMC model.

The steady-state and partial-equilibrium approximations use a different set of species and reactions for each process in Figure 2. The species and reactions were selected using a combination of techniques. A path flux analysis of the ABF mechanism [2] combined with a systematic inspection of reaction rates was used to determine important reactions to include for each process. Reactions that did not contribute significantly were excluded. Likewise, the intermediates that took part in these reactions were also excluded. The full sets of species and reactions used for each process are detailed in Appendix A.2.

4 Results and discussion

In the sections that follow we study the range of validity of the steady-state and partial-equilibrium approximations in models of PAH growth. In Section 4.1 we critically assess the performance of the steady-state approximation in simulations of a closed isothermal systems at different temperatures and equivalence ratios. In Section 4.2 we apply the partial-equilibrium approximation to the same systems and assess its performance versus that of the steady-state approximation. In Section 4.3, we introduce and investigate the performance of a new combined steady-state–partial-equilibrium approximation. Finally, in Section 4.4, we demonstrate the application of the new combined approximation in a KMC simulation of the PAH chemistry in a premixed burner-stabilised flame.

4.1 Steady-state approximation

In this section we study the case where all PAH species participating in the ring growth reactions, including intermediates and products, are in steady-state with the reactants.

In the case of the formation of naphthalene from benzene, Figure 2 process (i), benzene is considered to be a slow species while naphthalene and all its intermediates are included in the steady-state species set. In the case of the formation of phenanthrene from naphthalene, Figure 2 process (ii), naphthalene is considered to be a slow species while phenanthrene and its intermediates are included in the steady-state species set. The full set of species and reactions used for the steady-state approximation of each process is shown in Tables A.1 and A.2 in Appendix A.2. The ring condensation, Figure 2 process (iii), is not included in the steady-state approximation because it includes a reaction that is non-linear in the sense that it involves the reaction of two PAHs (Table A.3, reaction 17)-. This cannot be included in a steady-state approximation based on linear equations (*c.f.* Equation 1).

Figure 3 shows the concentrations of naphthalene and phenanthrene calculated using the steady-state approximation versus reference solutions calculated using the full ABF mechanism in a closed isothermal system. For simplicity, only one equivalence ratio and four temperatures are shown. The shaded area in the figure shows the range of residence times relevant to the production of PAHs in a typical flame. The figure shows that the state-state approximation closely matches the reference solutions at temperatures above 2000 K. However, at lower temperatures the method shows significant differences from the reference solution at short times. The difference decreases with time (and given long enough, good agreement is seen at all temperatures, see Appendix A.3). This is a well known feature of the steady-state approximation. The fast species need an *induction time*, which is a function of the lifetime of the slowest species in the approximation [3, 76], to achieve their steady-state concentrations.

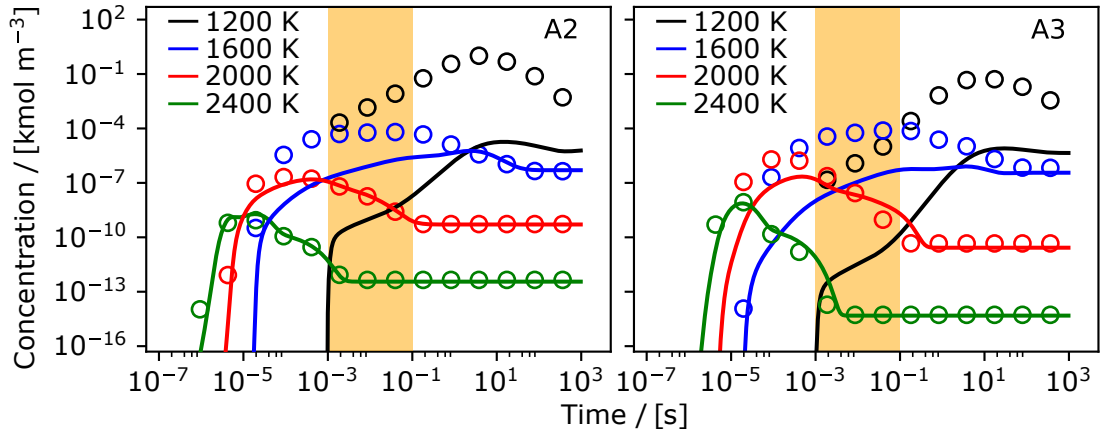


Figure 3: Simulations of the reaction of ethylene in a closed isothermal system, initially at an equivalence ratio of 5.0, to form naphthalene (A_2 , left panel) and phenanthrene (A_3 , right panel). Solid lines show the results of simulations using the full ABF mechanism. Circles show the concentration of each species calculated using the steady-state approximation. The shaded area shows typical flame residence times.

It is useful to define a metric to measure the quality of the steady-state approximation. However, an instantaneous measurement of the error can be misleading because PAHs are produced and consumed at different times under different conditions. For this reason, we introduce a time-integrated metric to provide information about the error over the timescales relevant to the study.

$$\varepsilon_{\alpha}^{\text{ss}}(\tau; \phi, T) = \log \left(\frac{\int_0^{\tau} c_{\alpha}^{\text{ss}}(t; \phi, T) dt}{\int_0^{\tau} c_{\alpha}^{\text{ref}}(t; \phi, T) dt} \right), \quad (2)$$

$$\hat{\varepsilon}_{\alpha}^{\text{ss}}(\tau; \phi, T) = \frac{|\varepsilon_{\alpha}^{\text{ss}}(\tau; \phi, T)|}{\max_{\phi, T}(\varepsilon_{\alpha}^{\text{ss}})},$$

where $\varepsilon_{\alpha}^{\text{ss}}(\tau; \phi, T)$ is the time-integrated error in the steady-state approximation of species α . It is computed as the logarithm of the ratio of the time integrals of c_{α}^{ss} , the concentration

of species α calculated using the steady-state approximation, and c_{α}^{ref} , the reference solution calculated using the full ABF mechanism. $\hat{\epsilon}_{\alpha}^{\text{ss}}(\tau; \phi, T)$ is normalised by the maximum error found over the temperature-equivalence ratio space. It must be noted that in these definitions we assume that the steady-state value is larger than the reference solution; a trend that we observed in all simulations but that may not be applicable to other systems.

Figure 4 shows a map of $\hat{\epsilon}_{\alpha}^{\text{ss}}(\tau = 1.0\text{s})$ versus temperature and equivalence ratio. The upper limit of the integral was selected as larger than the typical flame residence times to allow all significant errors to be captured by the time integral. The black lines show the location of a *soot island*, which is a region that is known to be important for soot emissions (in engine applications) [71]. It can be seen that errors accumulate at temperatures under 1700 K and equivalence ratios under 2.0, with some of these conditions being in the region relevant to soot formation.

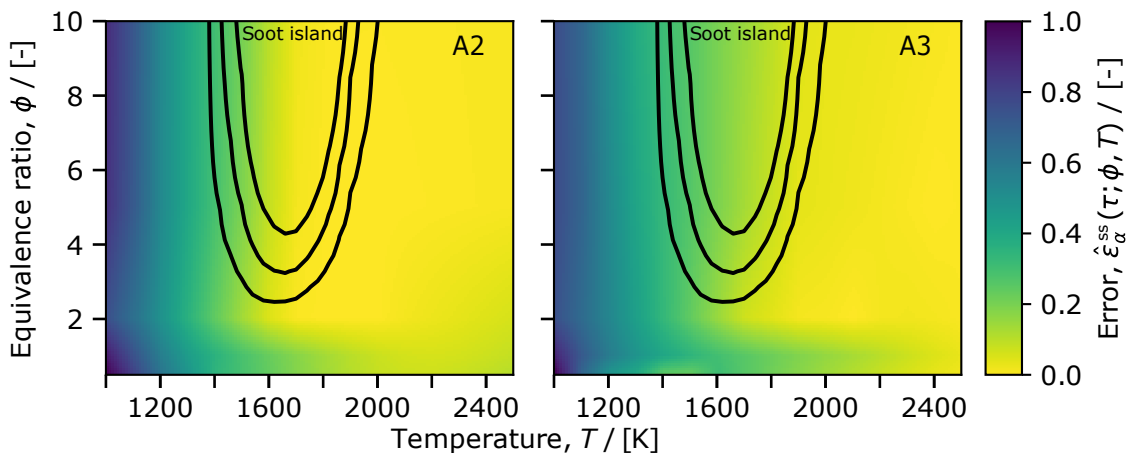


Figure 4: Time-integrated steady-state error $\hat{\epsilon}_{\alpha}^{\text{ss}}(\tau = 1.0\text{s})$ for the concentration of naphthalene (A_2 , left panel) and phenanthrene (A_3 , right panel) calculated via simulations of the reaction of ethylene in a closed isothermal system as a function of temperature and initial equivalence ratio and the concentration of each species calculated using the steady-state approximation. The black lines show the region that is most important for soot emissions (in engine applications) [71].

The concentrations of most intermediates follow the steady-state approximation under a wide range of conditions. However, species involved in the final ring-forming step (Table A.1, reactions 21–25 and Table A.2, reactions 15–16) deviate from this behaviour at the lower end of the temperature space in Figure 4. These include $A_1(\text{C}_2\text{H})\text{C}_2\text{H}_2^{\bullet}$, A_2^{\bullet} and A_2 which are involved in the formation of naphthalene, and $A_2(\text{C}_2\text{H})\text{C}_2\text{H}_2^{\bullet}$, A_3^{\bullet} and A_3 which are involved in the formation of phenanthrene.

During the induction time, these reactions progress much more quickly in the forward direction than in the reverse direction. The effect of this is that intermediate species are consumed by the forward reactions without being replenished by the reverse reactions. This is inconsistent with the steady-state approximation, which assumes that the rates of the forward and reverse reactions are approximately equal. This is the leading cause of the error shown in Figure 4.

4.2 Partial-equilibrium approximation

Most species investigated in the previous section are controlled by reactions where the forward and reverse rates are large compared to net rate of conversion to final product. However, some species, notably those responsible for the error shown in Figure 4, show a distinct induction period during which the forward (ring-forming) reactions proceed much more quickly than reverse (ring desorption) reactions. This difference in the time scales and the presence of an induction period suggest that the system might be amenable to a partial-equilibrium approximation. In this instance, our primary interest is whether this can improve the behaviour of the model during the induction period.

A set of partial-equilibrium species and reactions is proposed for each process shown in Figure 2. In the case of processes (i) and (ii), these are a subset of the steady-state sets. In the case of process (iii), the set excludes the non-linear reaction (Table A.3, reaction 17) that prevented the use of the steady-state approximation for this process in Section 4.1. The full set of species and reactions used for the partial-equilibrium approximation of each process is shown in Tables A.1–A.3 in Appendix A.2.

In each case, the partial-equilibrium approximation excludes the ring-forming reactions responsible for the formation of the final product PAHs A_2 and A_3 , and the corresponding radicals A_2^\bullet and A_3^\bullet . The concentrations of these species must be computed separately. The set of ODEs governing the concentrations of these species may be written in the form

$$\frac{dc_\alpha}{dt} = P_\alpha - L_\alpha c_\alpha, \quad (3)$$

where P_α is the rate of production of species α and L_α is a pseudo-first order rate constant for the loss of species α . During the induction period we expect the rate of production to be much greater than the rate of loss (due to the rates of the ring-forming versus ring desorption reactions). Whilst this condition holds, Equation (3) can be approximated as

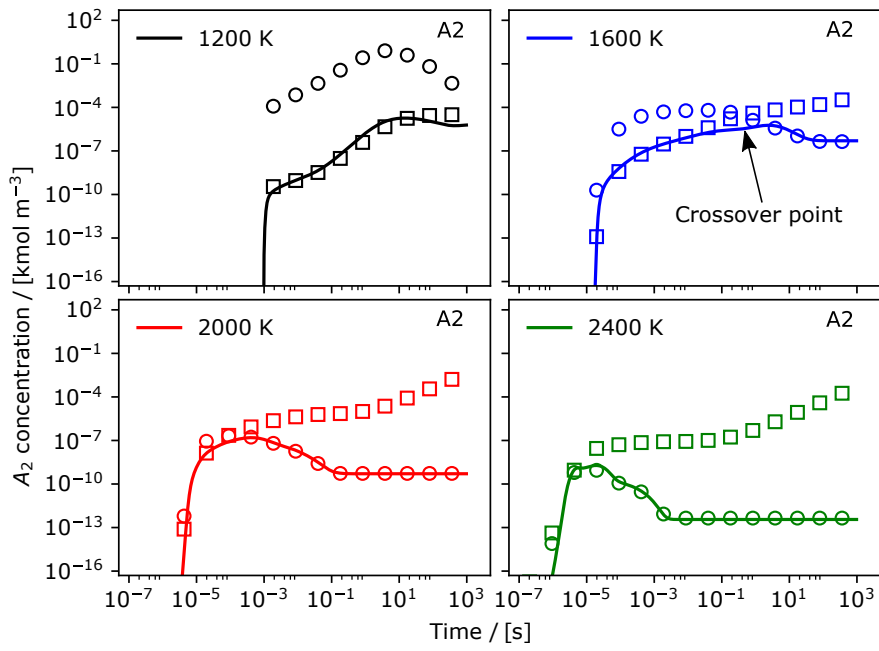
$$\frac{dc_\alpha}{dt} \approx P_\alpha,$$

and, noting that such that P_α is not a function of c_α ,

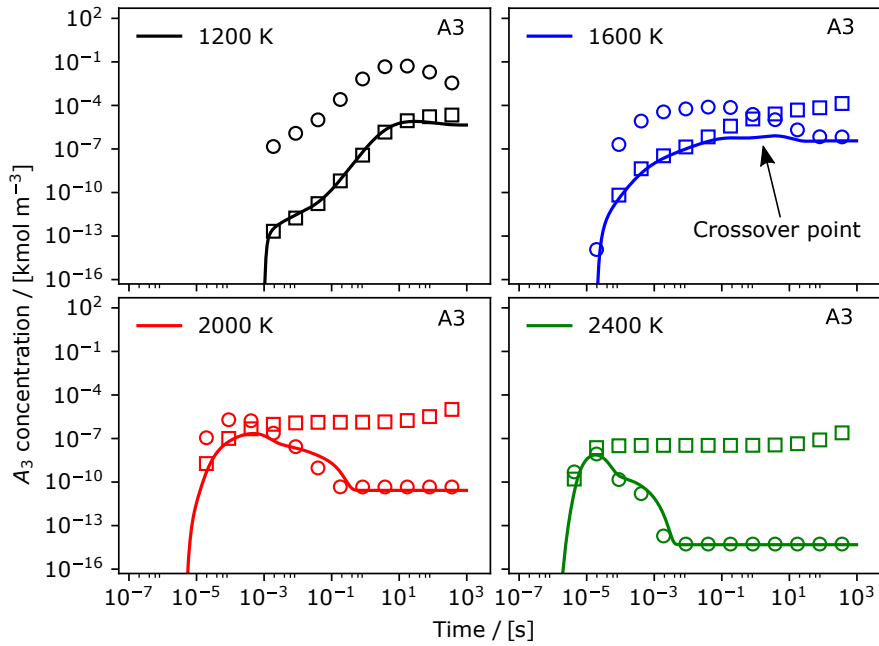
$$c_\alpha \approx \int_0^t P_\alpha dt. \quad (4)$$

In the simulations that follow, it is assumed that $A_2 + A_2^\bullet$ and $A_3 + A_3^\bullet$ are close to equilibrium. Equations of the form of Equation (4) are solved for the total concentration of each species and its corresponding radical, $c_{A_2} + c_{A_2^\bullet}$ and $c_{A_3} + c_{A_3^\bullet}$. A detailed step-by-step explanation of the treatment of these equations and reactions is given in Appendix A.2.1.

Figure 5 shows the concentrations of naphthalene and phenanthrene calculated using the partial-equilibrium approximation versus reference solutions calculated using the full ABF mechanism in a closed isothermal system. For comparison, we also show data calculated using the steady-state approximation. The figure shows that the partial-equilibrium approximation performs better than the state-state approximation at low temperatures and at short times. This is because of the improved treatment of the reactions responsible for the induction period and the inclusion of process (iii) (see Appendix A.3).



(a) Naphthalene (A_2).



(b) Phenanthrene (A_3).

Figure 5: Simulations of the reaction of ethylene in a closed isothermal system, initially at an equivalence ratio of 5.0, to form naphthalene (A_2 , top panels) and phenanthrene (A_3 , bottom panels). Solid lines show the results of simulations using the full ABF mechanism. Circles show the concentration of each species calculated using the steady-state approximation. Squares show the concentration of each species calculated using the partial-equilibrium approximation.

At longer times, the partial-equilibrium approximation performs less well due to neglecting the loss term in Equation (3). In all cases, there is a crossover point after which the steady-state approximation performs better than the partial-equilibrium approximation. (The location of this point is a strong function of temperature. It is most obvious in the cases at 1600 K.) This crossover point can be exploited in models of PAH growth.

4.3 A combined steady-state–partial-equilibrium approximation

We propose a new method that seeks to combine the strengths of the steady-state and partial-equilibrium approximations. The idea is to use the partial-equilibrium approximation during the induction period, before switching to use the steady-state approximation after the crossover point identified in the previous section.

The steady-state and partial-equilibrium approximations are combined as follows:

1. Use the steady-state approximation to evaluate the product concentrations, in this case $c_{A_2}^{ss}$ and $c_{A_3}^{ss}$. See Section 4.1.
2. Use the partial-equilibrium approximation to evaluate the product concentrations, in this case $c_{A_2}^{peq}$ and $c_{A_3}^{peq}$. See Section 4.2.
3. Determine the combined steady-state–partial-equilibrium product concentrations

$$c_{A_2}^{ss-peq} = \begin{cases} c_{A_2}^{peq} & \text{if } \lambda (P_{A_2} + P_{A_2^*}) > (L_{A_2} c_{A_{23}} + L_{A_2^*} c_{A_2^*}), \\ c_{A_2}^{ss} & \text{otherwise,} \end{cases} \quad (5)$$

and

$$c_{A_3}^{ss-peq} = \begin{cases} c_{A_3}^{peq} & \text{if } \lambda (P_{A_3} + P_{A_3^*}) > (L_{A_3} c_{A_3} + L_{A_3^*} c_{A_3^*}), \\ c_{A_3}^{ss} & \text{otherwise,} \end{cases} \quad (6)$$

where λ is a positive real number acting as a multiplier.

The rationale behind the criteria to determine the crossover point is that the production terms will be greater than the loss terms during the induction period (see the discussion in Section 4.2), such that the method will choose the partial-equilibrium approximation. At later times as the system stabilises, the production and loss terms will be approximately equal such that method will choose the steady-state approximation.

The multiplier λ is a parameter of the method. Its purpose is to guard against the case that the system has stabilised such that the steady-state approximation is the desired choice, but the relative values of the production and loss terms are such that the method imprudently chooses the partial-equilibrium approximation. This was not observed here, and in all cases the value of the parameter was set as $\lambda = 1$. However, it could conceivably become important in the future, so is included for completeness.

Figure 6 shows the concentrations of naphthalene and phenanthrene calculated using the combined steady-state–partial-equilibrium approximation versus reference solutions calculated using the full ABF mechanism in a closed isothermal system. In contrast to the

cases when either the steady-state or partial-equilibrium approximations are applied in isolation, the figure shows that the combined steady-state–partial-equilibrium approximation performs well both at early times (so during the induction period) and at long time (so when the system approaches equilibrium). Unsurprisingly, the main point at which there is deviation from the reference solution is close to the crossover point. This is most obvious in the case at 1600 K and can be predicted from the data in Figure 5.

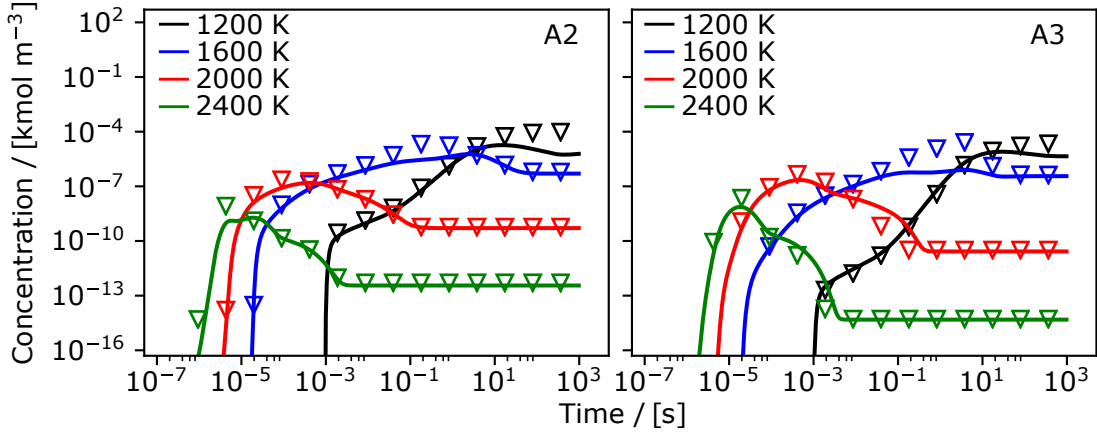


Figure 6: Simulations of the reaction of ethylene in a closed isothermal system, initially at an equivalence ratio of 5.0, to form naphthalene (A_2 , left panel) and phenanthrene (A_3 , right panel). Solid lines show the results of simulations using the full ABF mechanism. Triangles show the concentration of each species calculated using a combined steady-state and partial-equilibrium approximations.

In order to assess the accuracy of the combined steady-state–partial-equilibrium method, we define an error metric analogous to that in Equation (2)

$$\epsilon_{\alpha}^{\text{ss-peq}}(\tau; \phi, T) = \log \left(\frac{\int_0^{\tau} c_{\alpha}^{\text{ss-peq}}(t; \phi, T) dt}{\int_0^{\tau} c_{\alpha}^{\text{ref}}(t; \phi, T) dt} \right), \quad (7)$$

$$\hat{\epsilon}_{\alpha}^{\text{ss-peq}}(\tau; \phi, T) = \frac{|\epsilon_{\alpha}^{\text{ss-peq}}(\tau; \phi, T)|}{\max_{\phi, T}(\epsilon_{\alpha}^{\text{ss}})}.$$

$\hat{\epsilon}_{\alpha}^{\text{ss-peq}}(\tau; \phi, T)$ is normalised by the maximum error found over the temperature–equivalence ratio space for the *steady-state approximation*. This choice is deliberate and is intended to enable a direct comparison between errors calculated using Equations (2) and (7).

Figure 7 shows a map of $\hat{\epsilon}_{\alpha}^{\text{ss-peq}}(\tau = 1.0\text{s})$ versus temperature and equivalence ratio. A comparison with Figure 4 shows that the combined steady-state–partial-equilibrium performs much better than the steady-state assumption applied in isolation. In particular, at low temperatures and low equivalence ratios.

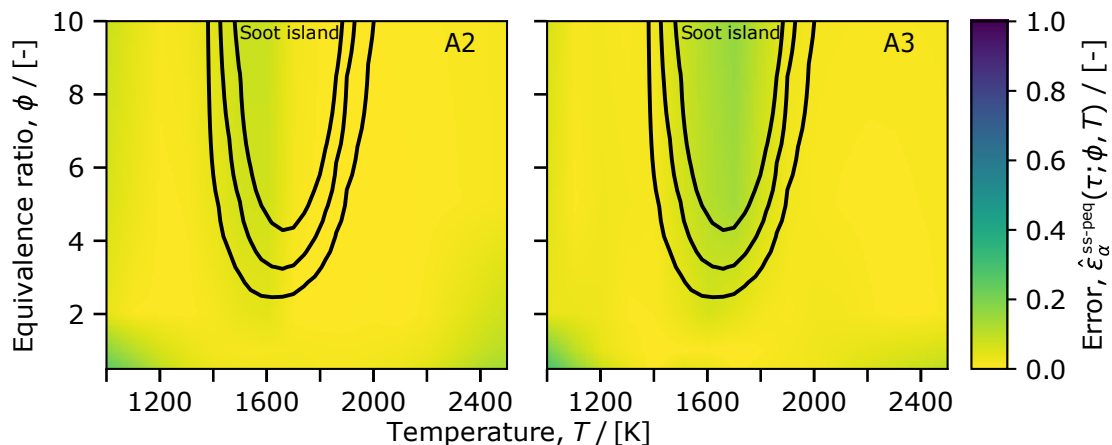


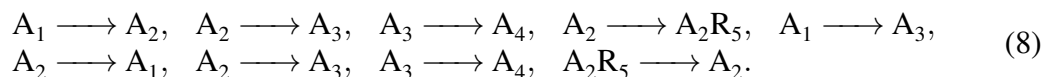
Figure 7: Time-integrated steady-state-partial-equilibrium error $\hat{\epsilon}_{\alpha}^{ss-peq}(\tau = 1.0s)$ for the concentration of naphthalene (A_2 , left panel) and phenanthrene (A_3 , right panel) calculated via simulations of the reaction of ethylene in a closed isothermal system as a function of temperature and initial equivalence ratio and the concentration of each species calculated using the combined steady-state and partial-equilibrium approximation. The black lines show the region that is most important for soot emissions (in engine applications) [71].

4.4 A combined steady-state-partial-equilibrium KMC model

In this section, we demonstrate the application of the combined steady-state-partial-equilibrium methodology to KMC simulations of PAH growth in a premixed burner-stabilised ethylene-oxygen flame at an equivalence ratio of 2.4. The simulations are based on the flame studied by Ciajolo et al. [14], albeit at range of cold-gas flow velocities in order to vary the transition point between the steady-state and partial-equilibrium approximations.

A fully-coupled simulation of the flame using the full ABF mechanism was used to obtain reference data for the species concentrations and temperature. The KMC simulations were performed as a Lagrangian post process, where the temperature and small-molecule concentrations (up to and including benzene, A_1) from the fully-coupled simulation were imposed as boundary conditions.

The following sequence of jump processes were included in the KMC model



This is a superset of the processes in Sections 4.1–4.3. The sequence is truncated at A_4 to maintain consistency with the ABF mechanism for the purpose of testing. The jump processes exist in pairs (for example, $A_1 \rightarrow A_2$ and $A_2 \rightarrow A_1$). This is important to ensure consistency with the underlying chemistry, in this case the ABF mechanism. The $A_3 \rightarrow A_1$ process is an exception and is omitted because its rate was negligible. The full set of species and reactions for each jump process is given in Table A.4 in Appendix A.2.

The combined steady-state–partial-equilibrium approximation method is modified to accommodate the new jump processes and to reflect the fact that the KMC model requires the method to return a set of rates as opposed to a concentrations

1. Use the steady-state approximation to evaluate the rate of each jump process.
2. Use the partial-equilibrium approximation to evaluate the rate of each jump process.
3. Determine the combined steady-state–partial-equilibrium approximation rates

$$r_{A_1 \rightarrow A_2}^{ss-peq} = \begin{cases} r_{A_1 \rightarrow A_2}^{peq} & \text{if } \lambda r_{A_1 \rightarrow A_2}^{peq} > r_{A_2 \rightarrow A_1}, \\ r_{A_1 \rightarrow A_2}^{ss} & \text{otherwise,} \end{cases} \quad (9)$$

$$r_{A_2 \rightarrow A_3}^{ss-peq} = \begin{cases} r_{A_2 \rightarrow A_3}^{peq} & \text{if } \lambda r_{A_2 \rightarrow A_3}^{peq} > r_{A_3 \rightarrow A_2}, \\ r_{A_2 \rightarrow A_3}^{ss} & \text{otherwise,} \end{cases} \quad (10)$$

$$r_{A_3 \rightarrow A_4}^{ss-peq} = \begin{cases} r_{A_3 \rightarrow A_4}^{peq} & \text{if } \lambda r_{A_3 \rightarrow A_4}^{peq} > r_{A_4 \rightarrow A_3}, \\ r_{A_3 \rightarrow A_4}^{ss} & \text{otherwise,} \end{cases} \quad (11)$$

$$r_{A_2 \rightarrow A_2 R_5}^{ss-peq} = \begin{cases} r_{A_2 \rightarrow A_2 R_5}^{peq} & \text{if } \lambda r_{A_2 \rightarrow A_2 R_5}^{peq} > r_{A_2 R_5 \rightarrow A_2}, \\ r_{A_2 \rightarrow A_2 R_5}^{ss} & \text{otherwise,} \end{cases} \quad (12)$$

and

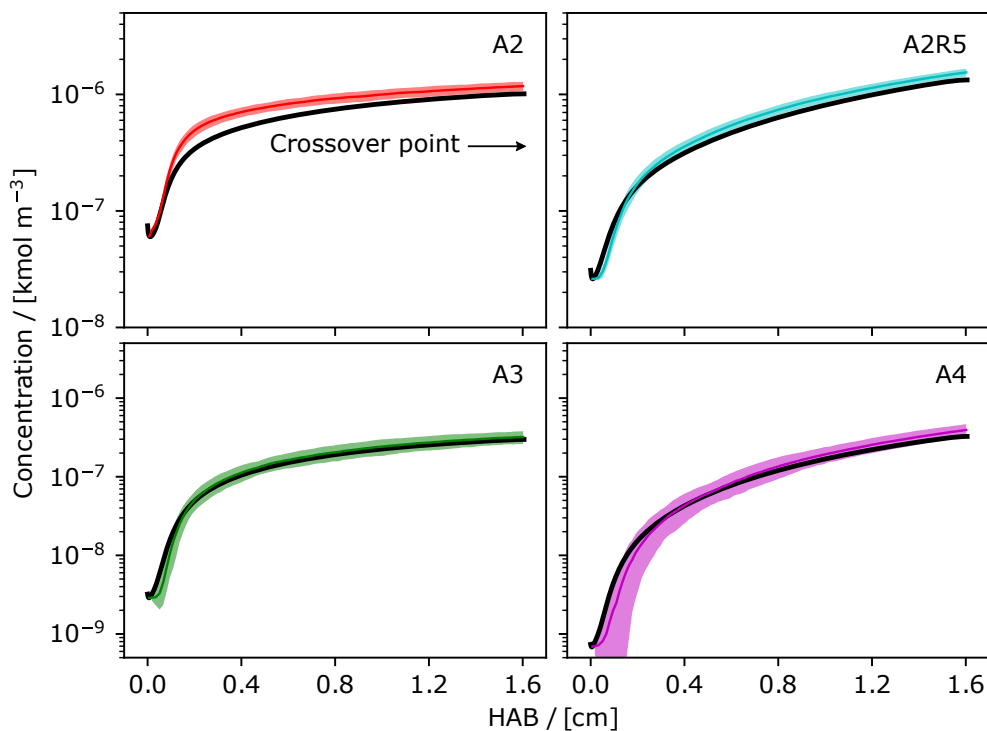
$$r_{A_1 \rightarrow A_3}^{ss-peq} = r_{A_1 \rightarrow A_3}^{peq} \quad \text{always,} \quad (13)$$

where r denotes the rate of a jump process. The calculated steady-state–partial-equilibrium rates r^{ss-peq} are used to determine which processes occur in the KMC simulation, which in turn calculates the concentrations of the final products, A_2 , A_3 , A_4 and $A_2 R_5$.

Note that the desorption processes (bottom row of Equation 8 and right-hand side of the inequalities in Equations 9–12) do not carry an ‘ss’ or ‘peq’ label because the rates of these processes are not a function of the species concentrations calculated via the steady-state or partial-equilibrium approximations. These rates are therefore calculated without either approximation. The rate of the $A_1 \rightarrow A_3$ process was taken from the partial-equilibrium approximation because the process cannot be described using the steady-state assumption (because of the non-linear reaction, Table A.3, reaction 17). The value of the multiplier was set as $\lambda = 1$ for all cases. A detailed step-by-step explanation of the treatment of the jump processes and reactions is given in Appendix A.2.2.

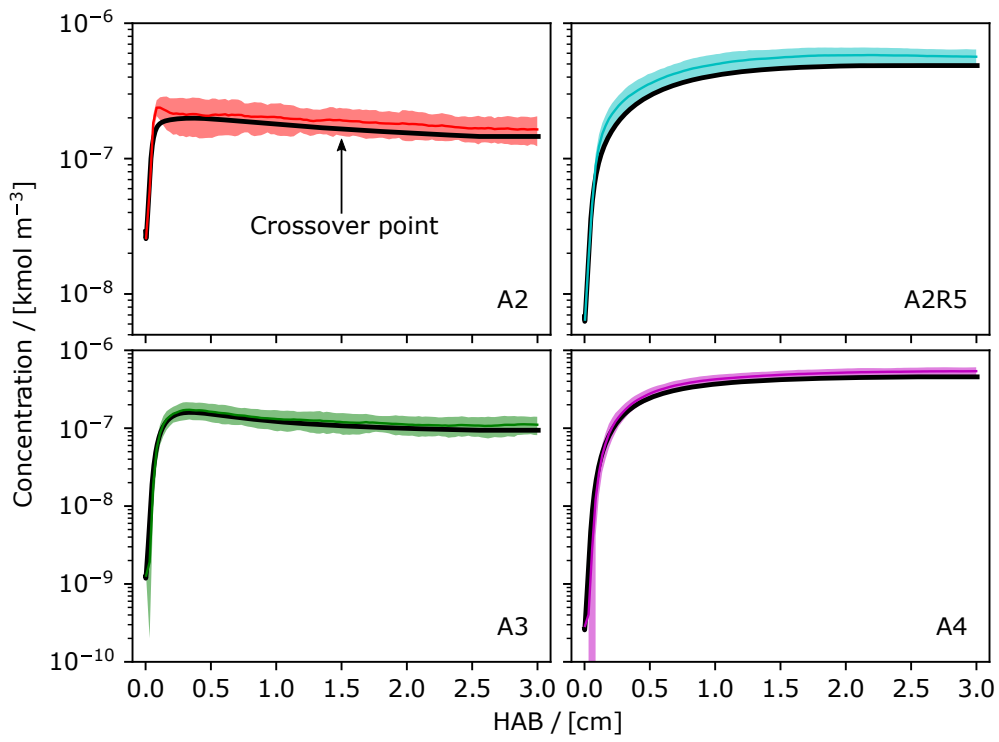
Figure 8 shows the concentrations of the products A_2 , A_3 , A_4 and $A_2 R_5$ calculated by the KMC model using the combined steady-state–partial-equilibrium approximation versus reference solutions calculated using the full ABF mechanism. The KMC model shows substantial agreement with the reference data. The main deviations occur in the concentration of A_2 before the crossover point in Figure 8(a) (where the model uses the partial-equilibrium approximation) and in the concentrations of A_3 and A_4 after the crossover point in Figure 8(c) (where the model uses the steady-state approximation) and are due to the approximate treatment of the chemistry. The relationship between the differences and the cold-gas flow velocity remains to be investigated.

The methodology demonstrated in Figure 8 allows KMC simulations of PAH growth in flame environments without introducing significant additional complexity. This is achieved by approximating the contributions of key intermediate species to the main PAH growth processes. Although the intermediate species may be of interest for some applications, we propose this combined steady-state and partial-equilibrium methodology for use in coupled simulations of PAH growth leading to soot (or other carbonaceous particle) formation, where it is necessary for the model to simulate a large ensemble of PAHs.

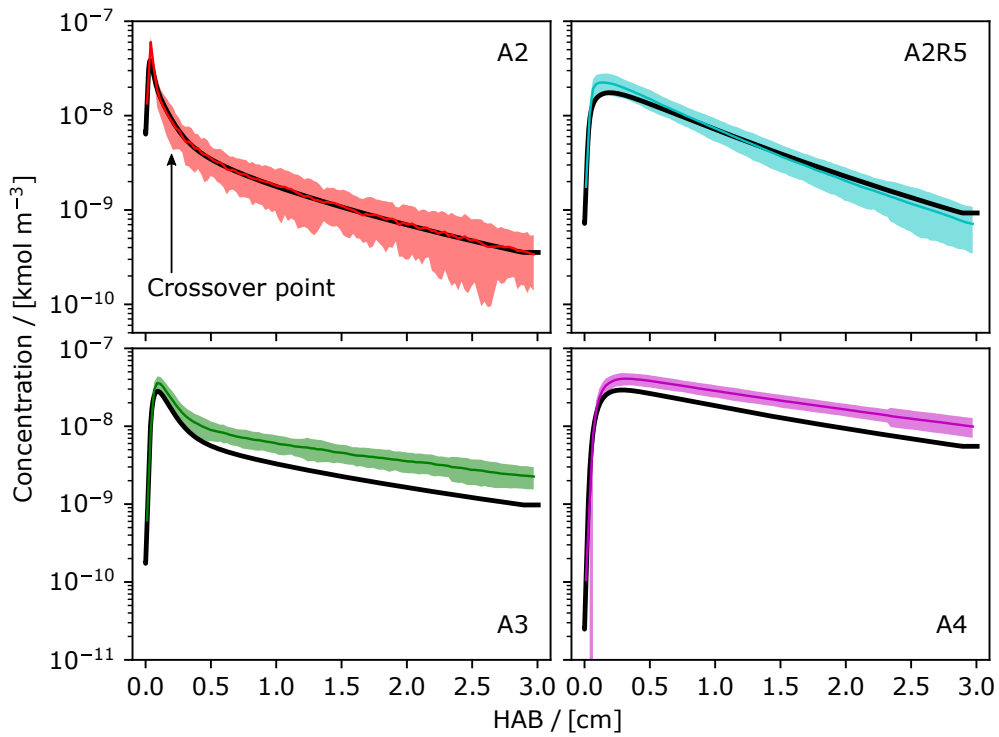


(a) Cold-gas flow velocity of 4 cm/s [as per 14].

Figure 8: Simulations of a premixed burner-stabilized ethylene flame at an equivalence ratio of 2.4 [14] to form naphthalene (A_2 , top left), acenaphthylene (A_2R_5 , top right), phenanthrene (A_3 , bottom left) and pyrene (A_4 , bottom right). Solid black lines show the results of fully-coupled flame simulations using the full ABF mechanism. Coloured lines show the average result from 100 KMC simulations using a combination of the steady-state and partial-equilibrium approximations. The coloured shaded region surrounding the lines shows two standard deviations to either side of the average KMC results. Part 1.



(b) Cold-gas flow velocity of 12 cm/s.



(c) Cold-gas flow velocity of 24 cm/s.

Figure 8: Simulations of a premixed burner-stabilized ethylene flame. Part 2.

5 Conclusions

This paper has investigated the range of validity of the steady-state and partial-equilibrium approximations for ring growth processes in the context of PAH-KMC models. These approximations were used to approximate the concentrations of intermediate species and express key growth pathways as jump processes. Simulations of closed systems showed that the steady-state approximation gave good results at high temperatures and long times, whereas the partial-equilibrium approximation gave good results at short times and low temperatures. A new methodology that combines both approximations was developed and tested in closed systems. The methodology compares the rate of partial-equilibrium growth with the rate of ring desorption to determine whether to use the steady-state or partial-equilibrium approximation. The methodology showed a substantial improvement in accuracy over the steady-state approximation across temperatures ranging from 1000 to 2500 K and equivalence ratios ranging from 0.5 to 10.

The proposed methodology was implemented in a KMC model of PAH growth to compute the growth rate of stochastic jump processes. The application of the model was demonstrated for simulations of a premixed ethylene flame. The results were in close agreement with a reference solution obtained from a fully-coupled simulation of the flame using the ABF mechanism. The ABF mechanism was selected because it contains well-established HACA sequences for PAH growth which are common to many later mechanisms and because it does not contain routes that are unique to small PAHs. This is an important requirement for generalising the KMC model developed in this work. The new methodology has the potential to be used to study the growth of large ensembles of PAHs, for example, in fully-coupled simulations of PAH growth and soot formation.

Acknowledgements

This work was partly funded by the National Research Foundation (NRF), Prime Minister's Office, Singapore under its Campus for Research Excellence and Technological Enterprise (CREATE) programme. This project has received funding from the European Union's Horizon 2020 research and innovation programme under Grant Agreement no. 724145. Gustavo Leon is funded by a CONACYT Cambridge Scholarship and wishes to acknowledge both institutions, the National Council of Science and Technology and the Cambridge Commonwealth Trust. Markus Kraft acknowledges the support of the Alexander von Humboldt foundation.

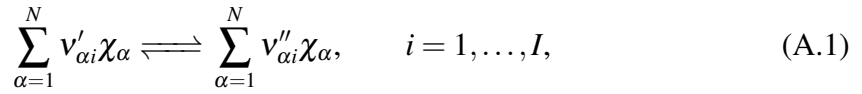
A Appendices

A.1 Steady-state and partial-equilibrium model equations

The sections that follow summarise the development of the steady-state and partial-equilibrium model equations used in this work. The exposition and the production and loss notation closely follows that used in a number of related works [see for example 31, 34, 37, 45, 76].

A.1.1 General reaction equations

A general set of chemical reactions can be written in the form



where χ are the chemical species and $v'_{\alpha i}$ and $v''_{\alpha i}$ are the forward and reverse stoichiometric coefficients of species α in reaction i . The rate of progress q_i can be written as

$$q_i = k_i \prod_{j=1}^N c_j^{v'_{ji}} - \frac{k_i}{K_{ci}} \prod_{j=1}^N c_j^{v''_{ji}}, \quad (\text{A.2})$$

where k_i is the forward rate constant, K_{ci} is the equilibrium constant of reaction i and c_j is the concentration of species j . The net production rate $\dot{\omega}_{\alpha}$ of species α is given as

$$\dot{\omega}_{\alpha} = \sum_{i=1}^I (v''_{\alpha i} - v'_{\alpha i}) q_i. \quad (\text{A.3})$$

A.1.2 Production and loss terms

The net production rate $\dot{\omega}_{\alpha}$ can be manipulated by substituting Equation (A.2) into Equation (A.3) to separate the terms responsible for the production and consumption of species α

$$\dot{\omega}_{\alpha} = \sum_{i=1}^I (v''_{\alpha i} - v'_{\alpha i}) \left(k_i \prod_{j=1}^N c_j^{v'_{ji}} - \frac{k_i}{K_{ci}} \prod_{j=1}^N c_j^{v''_{ji}} \right), \quad (\text{A.4})$$

$$\begin{aligned} &= \sum_{i=1}^I \left(v''_{\alpha i} k_i \prod_{j=1}^N c_j^{v'_{ji}} + v'_{\alpha i} \frac{k_i}{K_{ci}} \prod_{j=1}^N c_j^{v''_{ji}} \right) \\ &\quad - \sum_{i=1}^I \left(v'_{\alpha i} k_i \prod_{j=1}^N c_j^{v'_{ji}} + v''_{\alpha i} \frac{k_i}{K_{ci}} \prod_{j=1}^N c_j^{v''_{ji}} \right). \end{aligned} \quad (\text{A.5})$$

Assuming that all reactions are first order with respect to all species in the forward and reverse reactions, Equation (A.5) can be rearranged to give

$$\dot{\omega}_{\alpha} = P_{\alpha} - L_{\alpha} c_{\alpha}, \quad (\text{A.6})$$

where P_α and L_α are the production and loss terms of species α

$$P_\alpha = \sum_{i=1}^I P_\alpha^{(i)}, \quad \text{where} \quad P_\alpha^{(i)} = v''_{\alpha i} k_i \prod_{j=1}^N c_j^{v'_{ji}} + v'_{\alpha i} \frac{k_i}{K_{ci}} \prod_{j=1}^N c_j^{v''_{ji}}, \quad (\text{A.7})$$

$$L_\alpha = \sum_{i=1}^I L_\alpha^{(i)}, \quad \text{where} \quad L_\alpha^{(i)} = v'_{\alpha i} k_i \prod_{\substack{j=1 \\ j \neq \alpha}}^N c_j^{v'_{ji}} + v''_{\alpha i} \frac{k_i}{K_{ci}} \prod_{\substack{j=1 \\ j \neq \alpha}}^N c_j^{v''_{ji}}. \quad (\text{A.8})$$

In order to assist the analysis in the following sections, it is useful to introduce the terms

$$P_{\alpha,\beta} = \sum_{i \in R_{\beta \rightarrow \alpha}} P_{\alpha,\beta}^{(i)}, \quad \text{where} \quad P_{\alpha,\beta}^{(i)} = v''_{\alpha i} k_i \prod_{\substack{j=1 \\ j \neq \beta}}^N c_j^{v'_{ji}} + v'_{\alpha i} \frac{k_i}{K_{ci}} \prod_{\substack{j=1 \\ j \neq \beta}}^N c_j^{v''_{ji}}. \quad (\text{A.9})$$

$R_{\beta \rightarrow \alpha}$ is the set of reactions that produce species α from species β . The term $P_{\alpha,\beta}$ is a pseudo first-order rate coefficient such that $P_{\alpha,\beta} c_\beta$ gives rate of production of species α from species β under the first-order assumption made above and under the provision that species α and β are on different sides of the reaction equation.¹

The loss term is a pseudo first-order rate coefficient and has a connection with the lifetime τ_α of species α

$$\tau_\alpha = \frac{1}{L_\alpha}, \quad (\text{A.10})$$

which has been shown to be related to the time for which a short-lived species is present in a reaction system [76].

A.1.3 Approximations based on timescale separation

In the analysis that follows, we assume a closed constant-volume isothermal system with N species and I chemical reactions. A material balance over the system yields

$$\frac{dc_\alpha}{dt} = P_\alpha - L_\alpha c_\alpha, \quad \alpha = 1, \dots, N, \quad (\text{A.11})$$

where the right hand side describes the net production rate of species α and follows from Equation (A.6), and c is the solution vector containing the molar concentrations of the species.

Steady-state approximation

The steady-state approximation decomposes equation (A.11) into the following equations

$$0 \approx P_\alpha - L_\alpha c_\alpha, \quad \alpha \in S_{\text{ss}}, \quad (\text{A.12})$$

$$\frac{dc_\alpha}{dt} = P_\alpha - L_\alpha c_\alpha, \quad \alpha \notin S_{\text{ss}}, \quad (\text{A.13})$$

¹Under these restrictions, $(v'_{\alpha i}, v'_{\beta i}, v''_{\alpha i}, v''_{\beta i}) = (0, 1, 1, 0)$ or $(1, 0, 0, 1)$.

where S_{ss} denotes a subset of species that evolve rapidly relative to the other species in the system. The underlying assumption is that these species reach a local steady-state, such that the left hand side of Equation (A.12) tends to zero over timescales much smaller than the timescales of Equation (A.13). Tikhonov's theorem [74, 75] states that the solution of Equations (A.12) and (A.13) approaches the solution of Equation (A.11) as the left hand side of (A.12) tends to zero.

Equation (A.12) can be written as

$$L_\alpha c_\alpha - \sum_{\beta \in S_{ss}} P_{\alpha,\beta} c_\beta = P_\alpha - \underbrace{\sum_{\beta \in S_{ss}} P_{\alpha,\beta} c_\beta}_{=: b_\alpha}, \quad \alpha \in S_{ss}. \quad (\text{A.14})$$

A key insight is that Equation (A.14) is linear in the concentrations of the species in S_{ss} if S_{ss} is chosen such that no more than one species from S_{ss} appears on any side of a reaction. To see this, we note that under the given constraint, L_α is not a function of c_α (see Equation A.8) and $P_{\alpha,\beta}$ is not a function of c_α or c_β (see Equation A.9 and note that $P_{\alpha,\beta}$ describes the *production* of species α , such that species α is not a reactant). Furthermore, b_α does not depend on the species in S_{ss} because the second term introduced on the right hand side of Equation (A.14) is designed to exactly subtract those dependencies from P_α .

Under these constraints, Equation (A.14) can be written as a linear system

$$M_{ss} c_{ss} = b_{ss}, \quad (\text{A.15})$$

where c_{ss} is a vector of the molar concentrations of the species in the set S_{ss} ,

$$M_{ss} = \begin{bmatrix} L_{\alpha_1} & -P_{\alpha_1,\alpha_2} & \dots & -P_{\alpha_1,\alpha_{N_{ss}}} \\ -P_{\alpha_2,\alpha_1} & L_{\alpha_2} & \dots & -P_{\alpha_2,\alpha_{N_{ss}}} \\ \vdots & \vdots & \ddots & \vdots \\ -P_{\alpha_{N_{ss}},\alpha_1} & -P_{\alpha_{N_{ss}},\alpha_2} & \dots & L_{\alpha_{N_{ss}}} \end{bmatrix} \quad \text{and} \quad b_{ss} = \begin{bmatrix} b_{\alpha_1} \\ b_{\alpha_2} \\ \vdots \\ b_{\alpha_{N_{ss}}} \end{bmatrix},$$

where α_i , $i = 1, \dots, N_{ss}$ is an enumeration of the species in the set S_{ss} and

$$b_\alpha = P_\alpha - \sum_{\beta \in S_{ss}} P_{\alpha,\beta} c_\beta. \quad (\text{A.16})$$

Equation (A.15) can be solved for the concentrations of the species in the set S_{ss} . The concentrations of the remaining species must be solved by integrating Equation (A.13). The solutions of these equations must be tightly coupled in order to obtain accurate results. This approach that allows the reduction of the dimension of the set of ODEs from N to $N - N_{ss}$, reducing the computational cost of the problem.

Several authors have investigated the application of the steady-state approximation to different systems [44, 55, 75, 76]. Its application to slow-forming species can produce significant errors, whereas good results can be achieved given appropriate selection of fast-forming species. The chemical lifetime of a species seems to be the best predictor to determine whether it can be approximated or not by the steady-state assumption [75].

Partial-equilibrium approximation

The partial-equilibrium approximation decomposes Equation (A.11) into two equations

$$\frac{dc_\alpha}{dt} = P_\alpha - L_\alpha c_\alpha, \quad \alpha \in S_{\text{peq}}, \quad (\text{A.17})$$

$$\frac{dc_\alpha}{dt} = P_\alpha - L_\alpha c_\alpha, \quad \alpha \notin S_{\text{peq}}, \quad (\text{A.18})$$

where S_{peq} denotes a subset of species whose concentrations are controlled by a set of reactions that rapidly approach equilibrium, R_{peq} . These should be reversible reactions where the forward and reverse rates are large and approximately equal, and where at least one species in the reaction (a reactant, a product or one of each) belongs to S_{peq} .

The terms in Equation (A.17) can be further decomposed

$$\frac{dc_\alpha}{dt} = (P_\alpha^{\text{peq}} + P_\alpha^{\text{neq}}) - (L_\alpha^{\text{peq}} + L_\alpha^{\text{neq}}) c_\alpha, \quad \alpha \in S_{\text{peq}}, \quad (\text{A.19})$$

where P_α^{peq} and L_α^{peq} denote the contribution from reactions in R_{peq} (and P_α^{neq} and L_α^{neq} denote contributions from the remaining reactions) to P_α and L_α , such that

$$0 \approx P_\alpha^{\text{peq}} - L_\alpha^{\text{peq}} c_\alpha, \quad \alpha \in S_{\text{peq}}. \quad (\text{A.20})$$

Under constraints analogous to those described in relation to Equation (A.14), Equation (A.20) can be used to obtain a linear system for c_{peq}

$$M_{\text{peq}} c_{\text{peq}} = b_{\text{peq}}, \quad (\text{A.21})$$

where c_{peq} is a vector of the molar concentrations of the species in the set S_{peq} ,

$$M_{\text{peq}} = \begin{bmatrix} L_{\alpha_1}^{\text{peq}} & -P_{\alpha_1, \alpha_2}^{\text{peq}} & \cdots & -P_{\alpha_1, \alpha_{N_{\text{ss}}}}^{\text{peq}} \\ -P_{\alpha_2, \alpha_1}^{\text{peq}} & L_{\alpha_2}^{\text{peq}} & \cdots & -P_{\alpha_2, \alpha_{N_{\text{ss}}}}^{\text{peq}} \\ \vdots & \vdots & \ddots & \vdots \\ -P_{\alpha_{N_{\text{ss}}}, \alpha_1}^{\text{peq}} & -P_{\alpha_{N_{\text{ss}}}, \alpha_2}^{\text{peq}} & \cdots & L_{\alpha_{N_{\text{ss}}}}^{\text{peq}} \end{bmatrix} \quad \text{and} \quad b_{\text{peq}} = \begin{bmatrix} b_{\alpha_1}^{\text{peq}} \\ b_{\alpha_2}^{\text{peq}} \\ \vdots \\ b_{\alpha_{N_{\text{ss}}}}^{\text{peq}} \end{bmatrix},$$

where α_i , $i = 1, \dots, N_{\text{peq}}$ is an enumeration of the species in the set S_{peq} ,

$$b_\alpha^{\text{peq}} = P_\alpha^{\text{peq}} - \sum_{\beta \in S_{\text{peq}}} P_{\alpha, \beta}^{\text{peq}} c_\beta, \quad (\text{A.22})$$

and P_α^{peq} , L_α^{peq} and $P_{\alpha, \beta}^{\text{peq}}$ are defined as special cases of Equations (A.7), (A.8) and (A.9)

$$P_\alpha^{\text{peq}} = \sum_{i \in R_{\text{peq}}} P_\alpha^{(i)}, \quad (\text{A.23})$$

$$L_\alpha^{\text{peq}} = \sum_{i \in R_{\text{peq}}} L_\alpha^{(i)}, \quad (\text{A.24})$$

and

$$P_{\alpha, \beta}^{\text{peq}} = \sum_{i \in R_{\text{peq}} \cap R_{\beta \rightarrow \alpha}} P_{\alpha, \beta}^{(i)}, \quad (\text{A.25})$$

where the sum over reactions $i \in \mathbf{R}_{\text{peq}} \cap \mathbf{R}_{\beta \rightarrow \alpha}$ should be understood as a sum over the subset of reactions in \mathbf{R}_{peq} that produce species α from species β .

One important difference between the partial-equilibrium and steady-state approximations is that the terms in the partial-equilibrium Equations (A.23–A.25) are defined in terms of a subset of the reactions. One consequence of this is that the partial-equilibrium equations, (A.18) and (A.20), are less tightly coupled than the steady-state equations, (A.12) and (A.13).

A.2 Steady-state and partial-equilibrium reactions and species

Tables A.1–A.3 list the reactions and species used in steady-state and partial-equilibrium approximations in Sections 4.1–4.3 of the main text.

Table A.1: Reactions used for the steady-state and partial-equilibrium approximations of naphthalene (A_2) growing from benzene (A_1). Reactions above the midline (1–20) are used in the partial-equilibrium approximation. All reactions (1–28) are used in the steady-state approximation. The treatment of reactions 21–28 in the partial-equilibrium approximation is explained in Section A.2.1. Rates taken from ABF mechanism [2].

No.	Reaction				
1	A_1	+ H	\rightleftharpoons	A_1^\bullet	+ H_2
2	A_1	+ OH	\rightleftharpoons	A_1^\bullet	+ H_2O
3	A_1^\bullet	+ H + (M)	\rightleftharpoons	A_1	+ (M)
4	A_1^\bullet	+ C_2H_2	\rightleftharpoons	A_1C_2H	+ H
5	A_1^\bullet	+ C_2H_2	\rightleftharpoons	$A_1C_2H_2$	
6	A_1C_2H	+ H	\rightleftharpoons	$A_1C_2H_2$	
7	A_1C_2H	+ C_2H	\rightleftharpoons	$A_1(C_2H)C_2H_2$	+ H
8	A_1C_2H	+ H	\rightleftharpoons	$A_1C_2H^\bullet$	+ H_2
9	A_1C_2H	+ OH	\rightleftharpoons	$A_1C_2H^\bullet$	+ H_2O
10	$A_1C_2H^\bullet$	+ H + (M)	\rightleftharpoons	A_1C_2H	+ (M)
11	A_1	+ C_2H	\rightleftharpoons	A_1C_2H	+ H
12	$A_1C_2H_3$	+ H	\rightleftharpoons	$A_1C_2H_3^\bullet$	+ H_2
13	$A_1C_2H_3$	+ OH	\rightleftharpoons	$A_1C_2H_3^\bullet$	+ H_2O
14	$A_1C_2H_3^\bullet$	+ H + (M)	\rightleftharpoons	$A_1C_2H_3$	+ (M)
15	A_1^\bullet	+ C_2H_4	\rightleftharpoons	$A_1C_2H_3$	+ H
16	A_1^\bullet	+ C_2H_3	\rightleftharpoons	$A_1C_2H_3$	
17	A_1	+ C_2H_3	\rightleftharpoons	$A_1C_2H_3$	+ H
18	$A_1C_2H_3$	+ H	\rightleftharpoons	$A_1C_2H_2$	+ H_2
19	$A_1C_2H_3$	+ OH	\rightleftharpoons	$A_1C_2H_2$	+ H_2O
20	$A_1C_2H^\bullet$	+ C_2H_2	\rightleftharpoons	$A_1(C_2H)C_2H_2$	+ H
21 [†]	$A_1C_2H_2$	+ C_2H_2	\rightleftharpoons	A_2	+ H
22 [†]	$A_1C_2H_3^\bullet$	+ C_2H_2	\rightleftharpoons	A_2	+ H
23 [†]	A_1^\bullet	+ C_4H_4	\rightleftharpoons	A_2	+ H
24 [†]	$A_1C_2H^\bullet$	+ C_2H_2	\rightleftharpoons	A_2^\bullet	
25 [†]	$A_1(C_2H)C_2H_2^\bullet$	+ H	\rightleftharpoons	A_2^\bullet	
26	A_2	+ H	\rightleftharpoons	A_2^\bullet	+ H_2
27	A_2	+ OH	\rightleftharpoons	A_2^\bullet	+ H_2O
28	A_2^\bullet	+ H + (M)	\rightleftharpoons	A_2	+ (M)

[†] Indicates reactions contributing to Equation (A.30). See Section A.2.1.

Species sets:

$$S_{ss} = \{A_1^\bullet, A_1C_2H_2, A_1C_2H, A_1C_2H^\bullet, A_1C_2H_3, A_1C_2H_3^\bullet, A_1(C_2H)C_2H_2^\bullet, A_2^\bullet, A_2\}.$$

$$S_{peq} = \{A_1^\bullet, A_1C_2H_2, A_1C_2H, A_1C_2H^\bullet, A_1C_2H_3, A_1C_2H_3^\bullet, A_1(C_2H)C_2H_2^\bullet\}.$$

$$S_{ss} \setminus S_{peq} = \{A_2^\bullet, A_2\}.$$

Table A.2: Reactions used for the steady-state and partial-equilibrium approximations of phenanthrene (A_3) growing from naphthalene (A_2). Reactions above the mid-line (1–14) are used in the partial-equilibrium approximation. All reactions (1–19) are used in the steady-state approximation. The treatment of reactions 15–19 in the partial-equilibrium approximation is explained in Section A.2.1. Rates taken from ABF mechanism [2].

No.	Reaction				
1	A_2	$+ H$	\rightleftharpoons	A_2^\bullet	$+ H_2$
2	A_2	$+ OH$	\rightleftharpoons	A_2^\bullet	$+ H_2O$
3	A_2^\bullet	$+ H + (M)$	\rightleftharpoons	A_2	$+ (M)$
4	A_2^\bullet	$+ C_2H_2$	\rightleftharpoons	$A_2C_2H_2$	
5	A_2^\bullet	$+ C_2H_2$	\rightleftharpoons	A_2C_2H	$+ H$
6	A_2	$+ C_2H$	\rightleftharpoons	A_2C_2H	$+ H$
7	A_2C_2H	$+ H$	\rightleftharpoons	$A_2C_2H_2$	
8	$A_2C_2H_2$	$+ H$	\rightleftharpoons	A_2C_2H	$+ H_2$
9	$A_2C_2H_2$	$+ OH$	\rightleftharpoons	A_2C_2H	$+ H_2O$
10	A_2C_2H	$+ H$	\rightleftharpoons	$A_2C_2H^\bullet$	$+ H_2$
11	A_2C_2H	$+ OH$	\rightleftharpoons	$A_2C_2H^\bullet$	$+ H_2O$
12	$A_2C_2H^\bullet$	$+ H + (M)$	\rightleftharpoons	A_2C_2H	$+ (M)$
13	A_2C_2H	$+ C_2H$	\rightleftharpoons	$A_2(C_2H)C_2H_2$	$+ H$
14	$A_2C_2H^\bullet$	$+ C_2H_2$	\rightleftharpoons	$A_2(C_2H)C_2H_2$	$+ H$
15 [†]	$A_2C_2H^\bullet$	$+ C_2H_2$	\rightleftharpoons	A_3^\bullet	
16 [†]	$A_2(C_2H)C_2H_2^\bullet$	$+ H$	\rightleftharpoons	A_3^\bullet	
17	A_3	$+ H$	\rightleftharpoons	A_3^\bullet	$+ H_2$
18	A_3	$+ OH$	\rightleftharpoons	A_3^\bullet	$+ H_2O$
19	A_3^\bullet	$+ H + (M)$	\rightleftharpoons	A_3	$+ (M)$

[†] Indicates reactions contributing to Equation (A.30). See Section A.2.1.

Species sets:

$$S_{ss} = \{A_2^\bullet, A_2C_2H_2, A_2C_2H, A_2C_2H^\bullet, A_2(C_2H)C_2H_2^\bullet, A_3^\bullet, A_3\}.$$

$$S_{peq} = \{A_2^\bullet, A_2C_2H_2, A_2C_2H, A_2C_2H^\bullet, A_2(C_2H)C_2H_2^\bullet\}.$$

$$S_{ss} \setminus S_{peq} = \{A_3^\bullet, A_3\}.$$

Table A.3: Reactions used for partial-equilibrium approximation of phenanthrene (A_3) growing from benzene (A_1). Reactions above the midline (1–12) are used in the partial-equilibrium approximation. The treatment of reactions 13–17 is explained in Section A.2.1. Rates taken from ABF mechanism [2].

No.	Reaction				
1	A_1	$+ H$	\rightleftharpoons	A_1^\bullet	$+ H_2$
2	A_1	$+ OH$	\rightleftharpoons	A_1^\bullet	$+ H_2O$
3	A_1^\bullet	$+ H + (M)$	\rightleftharpoons	A_1	$+ (M)$
4	A_1^\bullet	$+ C_2H_2$	\rightleftharpoons	A_1C_2H	$+ H$
5	A_1^\bullet	$+ C_2H_2$	\rightleftharpoons	$A_1C_2H_2$	
6	A_1C_2H	$+ H$	\rightleftharpoons	$A_1C_2H_2$	
7	A_1C_2H	$+ C_2H$	\rightleftharpoons	$A_1(C_2H)C_2H_2$	$+ H$
8	A_1C_2H	$+ H$	\rightleftharpoons	$A_1C_2H^\bullet$	$+ H_2$
9	A_1C_2H	$+ OH$	\rightleftharpoons	$A_1C_2H^\bullet$	$+ H_2O$
10	$A_1C_2H^\bullet$	$+ H + (M)$	\rightleftharpoons	A_1C_2H	$+ (M)$
11	A_1	$+ C_2H$	\rightleftharpoons	A_1C_2H	$+ H$
12	$A_1C_2H^\bullet$	$+ C_2H_2$	\rightleftharpoons	$A_1(C_2H)C_2H_2$	$+ H$
13	A_1	$+ A_1^\bullet$	\rightleftharpoons	P_2	$+ H$
14	P_2	$+ H$	\rightleftharpoons	P_2^\bullet	$+ H_2$
15 [†]	P_2^\bullet	$+ C_2H_2$	\rightleftharpoons	A_3	$+ H$
16 [†]	A_1	$+ A_1C_2H^\bullet$	\rightleftharpoons	A_3	$+ H$
17 [†]	A_1^\bullet	$+ A_1C_2H$	\rightleftharpoons	A_3	$+ H$

[†] Indicates reactions contributing to Equation (A.30). See Section A.2.1.

Species sets:

$$S_{\text{peq}} = \{A_1^\bullet, A_1C_2H_2, A_1C_2H, A_1C_2H^\bullet, A_1(C_2H)C_2H_2^\bullet\}.$$

This process is only treated using the partial-equilibrium approximation.

Table A.4: Jump processes, reactions and species for the KMC model. For each process, reactions above the midline are used in the partial-equilibrium approximation; all reactions (above and below the line) are used in the steady-state approximation. Reactions below the midline are used to calculate the overall rate of the process. See Section A.2.2. Rates taken from ABF mechanism [2].

Jump process	Intermediate reactions					
	1	A_1	$+ H$	\rightleftharpoons	A_1^\bullet	$+ H_2$
	2	A_1	$+ OH$	\rightleftharpoons	A_1^\bullet	$+ H_2O$
	3	A_1^\bullet	$+ H + (M)$	\rightleftharpoons	A_1	$+ (M)$
	4	A_1^\bullet	$+ C_2H_2$	\rightleftharpoons	A_1C_2H	$+ H$
	5	A_1^\bullet	$+ C_2H_2$	\rightleftharpoons	$A_1C_2H_2$	
	6	A_1C_2H	$+ H$	\rightleftharpoons	$A_1C_2H_2$	
	7	A_1C_2H	$+ C_2H$	\rightleftharpoons	$A_1(C_2H)C_2H_2$	$+ H$
	8	A_1C_2H	$+ H$	\rightleftharpoons	$A_1C_2H^\bullet$	$+ H_2$
	9	A_1C_2H	$+ OH$	\rightleftharpoons	$A_1C_2H^\bullet$	$+ H_2O$
	10	$A_1C_2H^\bullet$	$+ H + (M)$	\rightleftharpoons	A_1C_2H	$+ (M)$
	11	A_1	$+ C_2H$	\rightleftharpoons	A_1C_2H	$+ H$
	12	$A_1C_2H_3$	$+ H$	\rightleftharpoons	$A_1C_2H_3^\bullet$	$+ H_2$
	13	$A_1C_2H_3$	$+ OH$	\rightleftharpoons	$A_1C_2H_3^\bullet$	$+ H_2O$
	14	$A_1C_2H_3^\bullet$	$+ H + (M)$	\rightleftharpoons	$A_1C_2H_3$	$+ (M)$
Free-edge	15	A_1^\bullet	$+ C_2H_4$	\rightleftharpoons	$A_1C_2H_3$	$+ H$
ring growth	16	A_1^\bullet	$+ C_2H_3$	\rightleftharpoons	$A_1C_2H_3$	
$A_1 \longrightarrow A_2$	17	A_1	$+ C_2H_3$	\rightleftharpoons	$A_1C_2H_3$	$+ H$
	18	$A_1C_2H_3$	$+ H$	\rightleftharpoons	$A_1C_2H_2$	$+ H_2$
	19	$A_1C_2H_3$	$+ OH$	\rightleftharpoons	$A_1C_2H_2$	$+ H_2O$
	20	$A_1C_2H^\bullet$	$+ C_2H_2$	\rightleftharpoons	$A_1(C_2H)C_2H_2$	$+ H$
	21 [†]	$A_1C_2H_2$	$+ C_2H_2$	\longrightarrow	A_2	$+ H$
	22 [†]	$A_1C_2H_3^\bullet$	$+ C_2H_2$	\longrightarrow	A_2	$+ H$
	23 [†]	A_1^\bullet	$+ C_4H_4$	\longrightarrow	A_2	$+ H$
	24 [†]	$A_1C_2H^\bullet$	$+ C_2H_2$	\longrightarrow	A_2^\bullet	
	25 [†]	$A_1(C_2H)C_2H_2^\bullet$	$+ H$	\longrightarrow	A_2^\bullet	
$S_{ss} = \{A_1^\bullet, A_1C_2H_2, A_1C_2H, A_1C_2H^\bullet,$ $A_1C_2H_3, A_1C_2H_3^\bullet, A_1(C_2H)C_2H_2^\bullet, A_2^\bullet, A_2\}.$						
$S_{peq} = \{A_1^\bullet, A_1C_2H_2, A_1C_2H, A_1C_2H^\bullet, A_1C_2H_3, A_1C_2H_3^\bullet, A_1(C_2H)C_2H_2^\bullet\}.$						
$S_{ss} \setminus S_{peq} = \{A_2^\bullet, A_2\}.$						

Continued on next page

Table A.4 – continued from previous page

Jump process	Intermediate reactions					
Free-edge ring desorption ¹ $A_2 \longrightarrow A_1$	1	A_2	+ H	\rightleftharpoons	A_2^\bullet	+ H_2
	2	A_2	+ OH	\rightleftharpoons	A_2^\bullet	+ H_2O
	3	A_2^\bullet	+ H + (M)	\rightleftharpoons	A_2	+ (M)
	4 [‡]	A_2	+ H	\longrightarrow	$A_1C_2H_2$	+ C_2H_2
	5 [‡]	A_2	+ H	\longrightarrow	$A_1C_2H_3^\bullet$	+ C_2H_2
	6 [‡]	A_2	+ H	\longrightarrow	A_1^\bullet	+ C_4H_4
	7 [‡]	A_2^\bullet		\longrightarrow	$A_1C_2H^\bullet$	+ C_2H_2
	8 [‡]	A_2^\bullet		\longrightarrow	$A_1(C_2H)C_2H_2$	+ H
Free-edge ring growth $A_2 \longrightarrow A_3$	1	A_2	+ H	\rightleftharpoons	$A_2^\bullet + H_2$	
	2	A_2	+ OH	\rightleftharpoons	A_2^\bullet	+ H_2O
	3	A_2^\bullet	+ H + (M)	\rightleftharpoons	A_2	+ (M)
	4	A_2^\bullet	+ C_2H_2	\rightleftharpoons	$A_2C_2H_2$	
	5	A_2^\bullet	+ C_2H_2	\rightleftharpoons	A_2C_2H	+ H
	6	A_2	+ C_2H	\rightleftharpoons	A_2C_2H	+ H
	7	A_2C_2H	+ H	\rightleftharpoons	$A_2C_2H_2$	
	8	$A_2C_2H_2$	+ H	\rightleftharpoons	A_2C_2H	+ H_2
	9	$A_2C_2H_2$	+ OH	\rightleftharpoons	A_2C_2H	+ H_2O
	10	A_2C_2H	+ H	\rightleftharpoons	$A_2C_2H^\bullet$	+ H_2
	11	A_2C_2H	+ OH	\rightleftharpoons	$A_2C_2H^\bullet$	+ H_2O
	12	$A_2C_2H^\bullet$	+ H + (M)	\rightleftharpoons	A_2C_2H	+ (M)
	13	A_2C_2H	+ C_2H	\rightleftharpoons	$A_2(C_2H)C_2H_2$	+ H
	14	$A_2C_2H^\bullet$	+ C_2H_2	\rightleftharpoons	$A_2(C_2H)C_2H_2$	+ H
15 [†]	$A_2C_2H^\bullet$	+ C_2H_2	\longrightarrow	A_3^\bullet		
16 [†]	$A_2(C_2H)C_2H_2^\bullet$	+ H	\longrightarrow	A_3^\bullet		
$S_{ss} = \{A_2^\bullet, A_2C_2H_2, A_2C_2H, A_2C_2H^\bullet, A_2(C_2H)C_2H_2^\bullet, A_3^\bullet, A_3\}$. $S_{peq} = \{A_2^\bullet, A_2C_2H_2, A_2C_2H, A_2C_2H^\bullet, A_2(C_2H)C_2H_2^\bullet\}$. $S_{ss} \setminus S_{peq} = \{A_3^\bullet, A_3\}$.						
Free-edge ring desorption ¹ $A_3 \longrightarrow A_2$	1	A_3	+ H	\rightleftharpoons	A_3^\bullet	+ H_2
	2	A_3	+ OH	\rightleftharpoons	A_3^\bullet	+ H_2O
	3	A_3^\bullet	+ H + (M)	\rightleftharpoons	A_3	+ (M)
	4 [‡]	A_3^\bullet		\longrightarrow	$A_2C_2H^\bullet$	+ C_2H_2
	5 [‡]	A_3^\bullet		\longrightarrow	$A_2(C_2H)C_2H_2$	+ H

Continued on next page

Table A.4 – continued from previous page

Jump process		Intermediate reactions				
Armchair ring growth $A_3 \longrightarrow A_4$	1	A_3	$+ H$	\rightleftharpoons	A_3^\bullet	$+ H_2$
	2	A_3	$+ OH$	\rightleftharpoons	A_3^\bullet	$+ H_2O$
	3	A_3^\bullet	$+ H + (M)$	\rightleftharpoons	A_3	$+ (M)$
	4	A_3^\bullet	$+ C_2H_2$	\rightleftharpoons	$A_3C_2H_2$	
	5	A_3^\bullet	$+ C_2H_2$	\rightleftharpoons	A_3C_2H	$+ H$
	6	A_3	$+ C_2H$	\rightleftharpoons	A_3C_2H	$+ H$
	7	A_3C_2H	$+ H$	\rightleftharpoons	$A_3C_2H_2$	
	8 [†]	A_3^\bullet	$+ C_2H_2$	\longrightarrow	A_4	$+ H$
	9 [†]	A_3C_2H	$+ H$	\longrightarrow	A_4	$+ H$
	10 [†]	$A_3C_2H_2$		\longrightarrow	A_4	$+ H$
$S_{ss} = \{A_3^\bullet, A_3C_2H_2, A_3C_2H, A_4\}$. $S_{peq} = \{A_3^\bullet, A_3C_2H_2, A_3C_2H\}$. $S_{ss} \setminus S_{peq} = \{A_4\}$.						
Armchair desorption $A_4 \longrightarrow A_3$	1 [‡]	A_4	$+ H$	\longrightarrow	A_3^\bullet	$+ C_2H_2$
	2 [‡]	A_4	$+ H$	\longrightarrow	A_3C_2H	$+ H$
	3 [‡]	A_4	$+ H$	\longrightarrow	$A_3C_2H_2$	
Ring condensation $A_1 \longrightarrow A_3$	1	A_1	$+ H$	\rightleftharpoons	A_1^\bullet	$+ H_2$
	2	A_1	$+ OH$	\rightleftharpoons	A_1^\bullet	$+ H_2O$
	3	A_1^\bullet	$+ H + (M)$	\rightleftharpoons	A_1	$+ (M)$
	4	A_1^\bullet	$+ C_2H_2$	\rightleftharpoons	A_1C_2H	$+ H$
	5	A_1^\bullet	$+ C_2H_2$	\rightleftharpoons	$A_1C_2H_2$	
	6	A_1C_2H	$+ H$	\rightleftharpoons	$A_1C_2H_2$	
	7	A_1C_2H	$+ C_2H$	\rightleftharpoons	$A_1(C_2H)C_2H_2$	$+ H$
	8	A_1C_2H	$+ H$	\rightleftharpoons	$A_1C_2H^\bullet$	$+ H_2$
	9	A_1C_2H	$+ OH$	\rightleftharpoons	$A_1C_2H^\bullet$	$+ H_2O$
	10	$A_1C_2H^\bullet$	$+ H + (M)$	\rightleftharpoons	A_1C_2H	$+ (M)$
	11	A_1	$+ C_2H$	\rightleftharpoons	A_1C_2H	$+ H$
	12	$A_1C_2H^\bullet$	$+ C_2H_2$	\rightleftharpoons	$A_1(C_2H)C_2H_2$	$+ H$
	13	A_1	$+ A_1^\bullet$	\rightleftharpoons	P_2	$+ H$
	14	P_2	$+ H$	\rightleftharpoons	P_2^\bullet	$+ H_2$
	15*	P_2^\bullet	$+ C_2H_2$	\longrightarrow	A_3	$+ H$
	16*	A_1	$+ A_1C_2H^\bullet$	\longrightarrow	A_3	$+ H$
	17*	A_1^\bullet	$+ A_1C_2H$	\longrightarrow	A_3	$+ H$
$S_{peq} = \{A_1^\bullet, A_1C_2H_2, A_1C_2H, A_1C_2H^\bullet, A_1(C_2H)C_2H_2^\bullet\}$. This process is only treated using the partial-equilibrium approximation.						

Continued on next page

Table A.4 – continued from previous page

Jump process		Intermediate reactions				
	1	A_2	+ H	\rightleftharpoons	$A_2^\bullet + H_2$	
	2	A_2	+ OH	\rightleftharpoons	A_2^\bullet	+ H_2O
	3	A_2^\bullet	+ H + (M)	\rightleftharpoons	A_2	+ (M)
	4	A_2^\bullet	+ C_2H_2	\rightleftharpoons	$A_2C_2H_2$	
	5	A_2^\bullet	+ C_2H_2	\rightleftharpoons	A_2C_2H	+ H
	6	A_2	+ C_2H	\rightleftharpoons	A_2C_2H	+ H
	7	A_2C_2H	+ H	\rightleftharpoons	$A_2C_2H_2$	
	8	$A_2C_2H_2$	+ H	\rightleftharpoons	A_2C_2H	+ H_2
	9	$A_2C_2H_2$	+ OH	\rightleftharpoons	A_2C_2H	+ H_2O
Five-member ring growth at zig-zag $A_2 \longrightarrow A_2R_5$	10	A_2C_2H	+ H	\rightleftharpoons	$A_2C_2H^\bullet$	+ H_2
	11	A_2C_2H	+ OH	\rightleftharpoons	$A_2C_2H^\bullet$	+ H_2O
	12	$A_2C_2H^\bullet$	+ H + (M)	\rightleftharpoons	A_2C_2H	+ (M)
	13	A_2C_2H	+ C_2H	\rightleftharpoons	$A_2(C_2H)C_2H_2$	+ H
	14	$A_2C_2H^\bullet$	+ C_2H_2	\rightleftharpoons	$A_2(C_2H)C_2H_2$	+ H
	15 [†]	A_2^\bullet	+ C_2H_2	\longrightarrow	A_2R_5	+ H
	16 [†]	A_2C_2H	+ H	\longrightarrow	A_2R_5	+ H
	17 [†]	$A_2C_2H_2$		\longrightarrow	A_2R_5	+ H
$S_{ss} = \{A_2^\bullet, A_2C_2H_2, A_2C_2H, A_2C_2H^\bullet, A_2(C_2H)C_2H_2^\bullet, A_2R_5\}$. $S_{peq} = \{A_2^\bullet, A_2C_2H_2, A_2C_2H, A_2C_2H^\bullet, A_2(C_2H)C_2H_2^\bullet\}$. $S_{ss} \setminus S_{peq} = \{A_2R_5\}$.						
Five-member ring desorption ¹ $A_2R_5 \longrightarrow A_2$	1 [‡]	A_2R_5	+ H	\longrightarrow	A_2^\bullet	+ C_2H_2
	2 [‡]	A_2R_5	+ H	\longrightarrow	A_2C_2H	+ H
	3 [‡]	A_2R_5	+ H	\longrightarrow	$A_2C_2H_2$	

¹ The rates of the desorption processes are independent of the concentration of intermediate PAH species, and can therefore be evaluated without a steady-state or partial-equilibrium approximation.

^{†/‡} Reversible reactions whose forward and reverse contributions are split between jump processes. The reactions are still treated as reversible for the purpose of solving Equation (A.14) for c_{ss} .

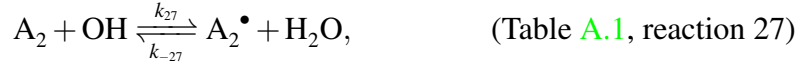
* Reactions treated as irreversible. The reverse rates were observed to be negligible.

^{†/‡/*} Reactions used to calculate the overall rate of each jump process. See Section A.2.2.

A.2.1 Treatment of non-partial-equilibrium reactions

The partial-equilibrium approximations in this work operate on a subset of reactions that exclude the formation of naphthalene (A_2 , Table A.1) and phenanthrene (A_3 , Tables A.2 and A.3). The concentrations of A_2 and A_3 must be calculated separately.

The concentrations of A_2 and A_3 are controlled by the final reactions in Tables A.1 and A.2



and



An algebraic relationship between the concentrations c_{A_2} and $c_{A_2^\bullet}$, and c_{A_3} and $c_{A_3^\bullet}$ can be derived by applying a steady-state or partial-equilibrium approximation to each of these sets of reactions [see for example 20]. In this work, a partial-equilibrium approximation is used to derive the following relationships

$$c_{A_2^\bullet} = c_{A_2} \left(\frac{k_{26}c_H + k_{27}c_{OH} + k_{-28}}{k_{-26}c_{H_2} + k_{-27}c_{H_2O} + k_{28}c_H} \right), \quad (\text{A.26})$$

$$c_{A_3^\bullet} = c_{A_3} \left(\frac{k_{17}c_H + k_{18}c_{OH} + k_{-19}}{k_{-17}c_{H_2} + k_{-18}c_{H_2O} + k_{19}c_H} \right). \quad (\text{A.27})$$

In the case of the ODE-based simulations (Sections 4.2 and 4.3), the concentrations of species in the set $\alpha \notin S_{\text{peq}}$ are calculated by solving Equation (A.18). The concentrations of the main PAH products, A_2 and A_3 , are treated as a special case and are calculated using Equations (A.26) and (A.27) in conjunction with solving equations of the same form as Equation (4) to find the total concentration of each species and its corresponding radical

$$c_{A_2} + c_{A_2^\bullet} \approx \int_0^t P_{A_2}^{\text{neq}} + P_{A_2^\bullet}^{\text{neq}} dt, \quad (\text{A.28})$$

$$c_{A_3} + c_{A_3^\bullet} \approx \int_0^t P_{A_3}^{\text{neq}} + P_{A_3^\bullet}^{\text{neq}} dt, \quad (\text{A.29})$$

where

$$P_\alpha^{\text{neq}} = \sum_{i \in R_{\text{neq}}} P_\alpha^{(i)}, \quad (\text{A.30})$$

is the production of species α due to the reactions in the set R_{neq} and $P_\alpha^{(i)}$ is defined as per Equation (A.7). The reactions in R_{neq} contributing to Equations (A.28) and (A.29) are marked with a dagger (\dagger) in Tables A.1–A.3. Note that Table A.3, reaction 17 has a dependency on the concentration of P_2^\bullet . This is evaluated using the relationship

$$c_{P_2} = \frac{k_{13}c_{A_1}c_{A_1^\bullet} + k_{-14}c_{P_2^\bullet}c_{H_2}}{k_{-13}c_H + k_{14}c_H} \quad (\text{A.31})$$

$$c_{P_2^\bullet} = \frac{k_{14}c_{P_2}c_H}{k_{-14}c_{H_2} + k_{15}c_{C_2H_2}} \quad (\text{A.32})$$

arising from the application of a steady-state approximation to Table A.3, reactions 13–15.

The rationale behind the special treatment of A_2 and A_3 is that it avoids the need to solve tightly coupled ODEs for the non-partial-equilibrium PAH species. This reduces the computational complexity of the method, so is desirable in the context of our objective to develop a computationally efficient model.

A.2.2 Calculation of KMC jump process rates

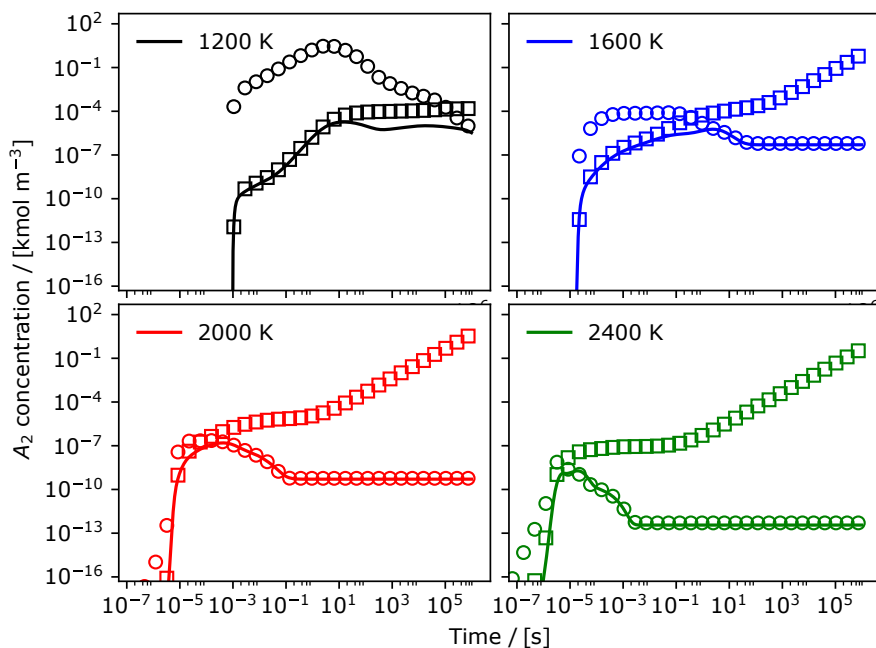
The KMC model calculates the concentrations of A_2 , A_2R_5 , A_3 and A_4 by performing a kinetic Monte Carlo simulation using the jump processes in Table A.4. The temperature and small-molecule concentrations (up to and including benzene, A_1) are imposed as boundary conditions. For each jump process, the concentrations of the (PAH) species in either S_{ss} or S_{peq} are calculated by solving Equation (A.15) for c_{ss} or Equation (A.21) for c_{peq} , depending on the choice of method. In both cases, the rates of the jump processes are calculated by evaluating the rates of the reactions marked \dagger , \ddagger and $*$ in Table A.4.

Similar to the treatment of the non-partial-equilibrium reactions in the ODE-based simulations (see Section A.2.1), the KMC model uses Equations (A.26) and (A.27) to calculate A_2 and A_3 in conjunction with tracking the total concentrations $c_{A_2} + c_{A_2^\bullet}$ and $c_{A_3} + c_{A_3^\bullet}$. Likewise, equations (A.31) and (A.32) are used to calculate the concentration of P_2^\bullet in order to evaluate the rate of the phenyl addition (Table A.4, reaction 15).

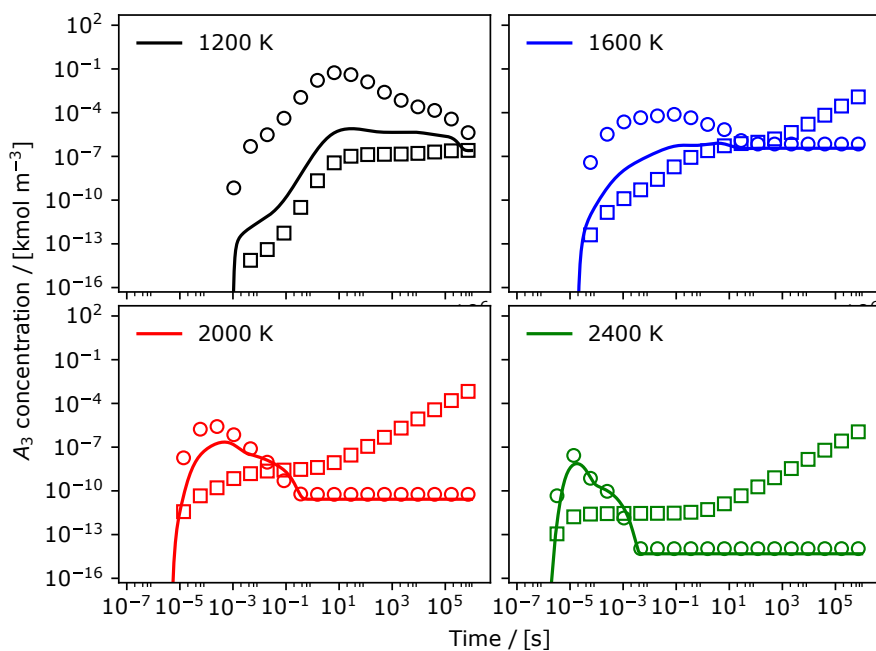
The mechanism in Table A.4 can be generalised (not shown here) to describe the growth of arbitrarily-sized PAHs. See for example the work by Frenklach and co-workers [20, 25] and Celnik et al. [10].

A.3 Effect of ring condensation reactions

Figure A.1 shows the concentrations of A_2 and A_3 calculated using the partial-equilibrium approximation without the inclusion of ring condensation reactions (Figure 2 process (iii) in the main text) versus reference solutions calculated using the full ABF mechanism in a closed isothermal system. For comparison, we also show data calculated using the steady-state approximation. The figure shows that given long enough, good agreement is seen between the steady-state approximation and the reference solutions. Comparison with Figure 5 (in the main text) shows that both the improved treatment of reactions during the induction period and the inclusion of process (iii) in the partial-equilibrium approximation are important to achieve agreement with the reference data for A_3 at early times.



(a) Naphthalene (A_2).



(b) Phenanthrene (A_3).

Figure A.1: Simulations of the reaction of ethylene in a closed isothermal system, initially at an equivalence ratio of 5.0, to form naphthalene (A_2 , top panels) and phenanthrene (A_3 , bottom panels). Solid lines show the results of simulations using the full ABF mechanism. Circles show the concentration of each species calculated using the steady-state approximation. Squares show the concentration of each species calculated using the partial-equilibrium approximation. Neither approximation includes process (iii).

References

- [1] E. Adkins and J. Miller. Extinction measurements for optical band gap determination of soot in a series of nitrogen-diluted ethylene/air non-premixed flames. *Physical Chemistry Chemical Physics*, 17(4):2686–95, 2015. doi:10.1039/c4cp04452e.
- [2] J. Appel, H. Bockhorn, and M. Frenklach. Kinetic modeling of soot formation with detailed chemistry and physics: Laminar premixed flames of C2 hydrocarbons. *Combustion and Flame*, 121(1-2):122–136, 2000. doi:10.1016/S0010-2180(99)00135-2.
- [3] S. W. Benson. The induction period in chain reactions. *The Journal of Chemical Physics*, 20(10):1605–1612, 1952. doi:10.1063/1.1700223.
- [4] G. P. Beretta, J. C. Keck, M. Janbozorgi, and H. Metghalchi. The rate-controlled constrained-equilibrium approach to far-from-local-equilibrium thermodynamics. *Entropy*, 14(2):92–130, 2012. doi:10.3390/e14020092.
- [5] G. Blanquart, P. Pepiot-Desjardins, and H. Pitsch. Chemical mechanism for high temperature combustion of engine relevant fuels with emphasis on soot precursors. *Combustion and Flame*, 156(3):588–607, 2009. doi:10.1016/j.combustflame.2008.12.007.
- [6] M. L. Botero, E. M. Adkins, S. González-Calera, H. Miller, and M. Kraft. PAH structure analysis of soot in a non-premixed flame using high-resolution transmission electron microscopy and optical band gap analysis. *Combustion and Flame*, 164:250–258, 2016. doi:https://doi.org/10.1016/j.combustflame.2015.11.022.
- [7] M. L. Botero, D. Chen, S. González-Calera, D. Jefferson, and M. Kraft. HRTEM evaluation of soot particles produced by the non-premixed combustion of liquid fuels. *Carbon*, 96:459–473, 2016. doi:https://doi.org/10.1016/j.carbon.2015.09.077.
- [8] M. L. Botero, N. Eaves, J. A. Dreyer, Y. Sheng, J. Akroyd, W. Yang, and M. Kraft. Experimental and numerical study of the evolution of soot primary particles in a diffusion flame. *Proceedings of the Combustion Institute*, 37(2):2047–2055, 2019. doi:10.1016/j.proci.2018.06.185.
- [9] M. Celnik, R. Patterson, M. Kraft, and W. Wagner. Coupling a stochastic soot population balance to gas-phase chemistry using operator splitting. *Combustion and Flame*, 148(3):158–176, 2007. ISSN 0010-2180. doi:10.1016/j.combustflame.2006.10.007.
- [10] M. Celnik, A. Raj, R. West, R. Patterson, and M. Kraft. Aromatic site description of soot particles. *Combustion and Flame*, 155(1-2):161–180, 2008. doi:10.1016/j.combustflame.2008.04.011.

- [11] M. Celnik, R. Patterson, M. Kraft, and W. Wagner. A predictor-corrector algorithm for the coupling of stiff odes to a particle population balance. *Journal of Computational Physics* 228, 2758-2769, (2009), 228(8):2758–2769, 2009. ISSN 0021-9991. doi:10.1016/j.jcp.2008.12.030.
- [12] D. Chen, Z. Zainuddin, E. Yapp, J. Akroyd, S. Mosbach, and M. Kraft. A fully coupled simulation of PAH and soot growth with a population balance model. *Proceedings of the Combustion Institute*, 34(1):1827–1835, 2013. doi:10.1016/j.proci.2012.06.089.
- [13] V. Chernov, M. J. Thomson, S. B. Dworkin, N. A. Slavinskaya, and U. Riedel. Soot formation with C1 and C2 fuels using an improved chemical mechanism for PAH growth. *Combustion and Flame*, 161(2):592–601, 2014. doi:10.1016/j.combustflame.2013.09.017.
- [14] A. Ciajolo, A. D’Anna, R. Barbella, A. Tregrossi, and A. Violi. The effect of temperature on soot inception in premixed ethylene flames. *Symposium (International) on Combustion*, 26(2):2327–2333, 1996. doi:10.1016/S0082-0784(96)80061-0.
- [15] M. B. Colket and D. J. Seery. Reaction mechanisms for toluene pyrolysis. *Symposium (International) on Combustion*, 25(1):883–891, 1994. doi:10.1016/S0082-0784(06)80723-X.
- [16] T. Dillstrom and A. Violi. The effect of reaction mechanisms on the formation of soot precursors in flames. *Combustion Theory and Modelling*, 21(1):23–34, 2017. doi:10.1080/13647830.2016.1211741.
- [17] N. A. Eaves, A. Veshkini, C. Riese, Q. Zhang, S. B. Dworkin, and M. J. Thomson. A numerical study of high pressure, laminar, sooting, ethane-air coflow diffusion flames. *Combustion and Flame*, 159(10):3179–3190, 2012. doi:10.1016/j.combustflame.2012.03.017.
- [18] P. Elvati, V. T. Dillstrom, and A. Violi. Oxygen driven soot formation. *Proceedings of the Combustion Institute*, 36(1):825–832, 2017. doi:10.1016/j.proci.2016.09.019.
- [19] M. Frenklach. On the driving force of PAH production. *Symposium (International) on Combustion*, 22(1):1075–1082, 1989.
- [20] M. Frenklach. On surface growth mechanism of soot particles. *Symposium (International) on Combustion*, 26(2):2285–2293, 1996. doi:10.1016/S0082-0784(96)80056-7.
- [21] M. Frenklach. Reaction mechanism of soot formation in flames. *Physical Chemistry Chemical Physics*, 4(11):2028–2037, 2002. doi:10.1039/b110045a.
- [22] M. Frenklach. New form for reduced modeling of soot oxidation: Accounting for multi-site kinetics and surface reactivity. *Combustion and Flame*, 201:148–159, 2019. doi:10.1016/j.combustflame.2018.12.023.

- [23] M. Frenklach and H. Wang. Detailed modeling of soot particle nucleation and growth. *Symposium (International) on Combustion*, 23(1):1559–1566, 1991. doi:10.1016/S0082-0784(06)80426-1.
- [24] M. Frenklach, W. Gardiner, S. Stein, D. Clary, and T. Yuan. Mechanism of soot formation in acetylene-oxygen mixtures. *Combustion Science and Technology*, 50(1-3):79–115, 1986. doi:10.1080/00102208608923927.
- [25] M. Frenklach, C. A. Schuetz, and J. Ping. Migration mechanism of aromatic-edge growth. *Proceedings of the Combustion Institute*, 30(1):1389–1396, 2005. doi:10.1016/j.proci.2004.07.048.
- [26] M. Frenklach, Z. Liu, R. I. Singh, G. R. Galimova, V. N. Azyazov, and A. M. Mebel. Detailed, sterically-resolved modeling of soot oxidation: Role of O atoms, interplay with particle nanostructure, and emergence of inner particle burning. *Combustion and Flame*, 188:284–306, 2018. doi:10.1016/j.combustflame.2017.10.012.
- [27] M. Frenklach, R. I. Singh, and A. M. Mebel. On the low-temperature limit of HACA. *Proceedings of the Combustion Institute*, 000:1–8, 2018. doi:10.1016/j.proci.2018.05.068.
- [28] D. T. Gillespie. A general method for numerically simulating the stochastic time evolution of coupled chemical reactions. *Journal of Computational Physics*, 22(4):403–434, 1976. doi:10.1016/0021-9991(76)90041-3.
- [29] A. N. Gorban. Model reduction in chemical dynamics: slow invariant manifolds, singular perturbations, thermodynamic estimates, and analysis of reaction graph. *Current Opinion in Chemical Engineering*, 21:48–59, 2018. doi:10.1016/j.coche.2018.02.009.
- [30] A. N. Gorban and I. V. Karlin. Method of invariant manifold for chemical kinetics. *Chemical Engineering Science*, 58(21):4751–4768, 2003. doi:10.1016/j.ces.2002.12.001.
- [31] D. A. Goussis. Quasi steady state and partial equilibrium approximations: Their relation and their validity. *Combustion Theory and Modelling*, 16(5):869–926, 2012. doi:10.1080/13647830.2012.680502.
- [32] D. A. Goussis and S.-H. Lam. A study of homogeneous methanol oxidation kinetics using CSP. *Symposium (International) on Combustion*, 24(1):113–120, 1992. doi:10.1016/S0082-0784(06)80018-4.
- [33] J. Happold, H.-H. Grotheer, and M. Aigner. Distinction of gaseous soot precursor molecules and soot precursor particles through photoionization mass spectrometry. *Rapid Communications in Mass Spectrometry*, 21(7):1247–1254, 2007. doi:10.1002/rcm.2955.
- [34] E. Hesstvedt, Ö. Hov, and I. S. A. Isaksen. Quasi-steady-state approximations in air pollution modeling: Comparison of two numerical schemes for oxidant prediction. *International Journal of Chemical Kinetics*, 10(9):971–994, 1978. doi:10.1002/kin.550100907.

- [35] D. Hou, C. S. Lindberg, M. Y. Manuputty, X. You, and M. Kraft. Modelling soot formation in a benchmark ethylene stagnation flame with a new detailed population balance model. *Combustion and Flame*, 203:56–71, 2019. doi:10.1016/j.combustflame.2019.01.035.
- [36] N. A. H. Janssen, G. Hoek, M. Simic-Lawson, P. Fischer, L. van Bree, H. ten Brink, M. Keuken, R. W. Atkinson, H. R. Anderson, B. Brunekreef, and F. R. Cassee. Black Carbon as an Additional Indicator of the Adverse Health Effects of Airborne Particles Compared with PM10 and PM2.5. *Environmental Health Perspectives*, 119(12):1691–1699, 2011. doi:10.1289/ehp.1003369.
- [37] L. Jay, A. Sandu, F. Potra, and G. Carmichael. Improved quasi-steady-state-approximation methods for atmospheric chemistry integration. *SIAM Journal on Scientific Computing*, 18(1):182–202, 1997. doi:10.1137/S1064827595283033.
- [38] K. O. Johansson, T. Dillstrom, P. Elvati, M. F. Campbell, P. E. Schrader, D. M. Popolan-Vaida, N. K. Richards-Henderson, K. R. Wilson, A. Violi, and H. A. Michelsen. Radical-radical reactions, pyrene nucleation, and incipient soot formation in combustion. *Proceedings of the Combustion Institute*, 36(1):799–806, 2017. doi:10.1016/j.proci.2016.07.130.
- [39] W. P. Jones and S. Rigopoulos. Rate-controlled constrained equilibrium: Formulation and application to nonpremixed laminar flames. *Combustion and Flame*, 142(3):223–234, 2005. doi:10.1016/j.combustflame.2005.03.008.
- [40] J. C. Keck and D. Gillespie. Rate-controlled partial-equilibrium method for treating reacting gas mixtures. *Combustion and Flame*, 17(2):237–241, 1971. doi:10.1016/S0010-2180(71)80166-9.
- [41] A. Khosousi and S. B. Dworkin. Soot surface reactivity during surface growth and oxidation in laminar diffusion flames. *Combustion and Flame*, 162(12):4523–4532, 2015. doi:10.1016/j.combustflame.2015.09.005.
- [42] K.-H. Kim, S. A. Jahan, E. Kabir, and R. J. Brown. A review of airborne polycyclic aromatic hydrocarbons (PAHs) and their human health effects. *Environment International*, 60:71–80, 2013. doi:https://doi.org/10.1016/j.envint.2013.07.019.
- [43] J. Y. W. Lai, P. Elvati, and A. Violi. Stochastic atomistic simulation of polycyclic aromatic hydrocarbon growth in combustion. *Physical Chemistry Chemical Physics*, 16(17):7969–7979, 2014. doi:10.1039/C4CP00112E.
- [44] C. K. Law. *Combustion Physics*. Cambridge University Press, 2006. doi:10.1017/CBO9780511754517.
- [45] T. Løvas, D. Nilsson, and F. Mauss. Automatic reduction procedure for chemical mechanisms applied to premixed methane/air flames. *Proceedings of the Combustion Institute*, 28(2):1809–1815, 2000. doi:10.1016/S0082-0784(00)80583-4.

- [46] P. J. Lupo, P. H. Langlois, J. Reefhuis, C. C. Lawson, E. Symanski, T. A. Desrosiers, Z. G. Khodr, A. J. Agopian, M. A. Waters, K. N. Duwe, R. H. Finnell, L. E. Mitchell, C. A. Moore, P. A. Romitti, and G. M. Shaw. Maternal occupational exposure to polycyclic aromatic hydrocarbons: Effects on gastroschisis among offspring in the national birth defects prevention study. *Environmental Health Perspectives*, 120(6): 910–915, 2012. doi:10.1289/ehp.1104305.
- [47] U. Maas and S. Pope. Simplifying chemical kinetics: Intrinsic low-dimensional manifolds in composition space. *Combustion and Flame*, 88(3):239–264, 1992. doi:10.1016/0010-2180(92)90034-M.
- [48] J. R. McConnell, R. Edwards, G. L. Kok, M. G. Flanner, C. S. Zender, E. S. Saltzman, J. R. Banta, D. R. Pasteris, M. M. Carter, and J. D. W. Kahl. 20th-century industrial black carbon emissions altered arctic climate forcing. *Science*, 317(5843): 1381–1384, 2007. doi:10.1126/science.1144856.
- [49] A. M. Mebel, Y. Georgievskii, A. W. Jasper, and S. J. Klippenstein. Temperature- and pressure-dependent rate coefficients for the HACA pathways from benzene to naphthalene. *Proceedings of the Combustion Institute*, 000:1–8, 2016. doi:10.1016/j.proci.2016.07.013.
- [50] R. S. Mehta, D. C. Haworth, and M. F. Modest. An assessment of gas-phase reaction mechanisms and soot models for laminar atmospheric-pressure ethylene-air flames. *Proceedings of the Combustion Institute*, 32(1):1327–1334, 2009. doi:10.1016/j.proci.2008.06.149.
- [51] J. H. Miller, J. D. Herdman, C. D. Green, and E. M. Webster. Experimental and computational determinations of optical band gaps for PAH and soot in a N₂-diluted, ethylene/air non-premixed flame. *Proceedings of the Combustion Institute*, 34(2):3669–3675, 2013. ISSN 1540-7489. doi:https://doi.org/10.1016/j.proci.2012.05.054.
- [52] N. W. Moriarty and M. Frenklach. Ab initio study of naphthalene formation by addition of vinylacetylene to phenyl. *Proceedings of the Combustion Institute*, 28(2):2563–2568, 2000. doi:10.1016/S0082-0784(00)80673-6.
- [53] K. Narayanaswamy, G. Blanquart, and H. Pitsch. A consistent chemical mechanism for oxidation of substituted aromatic species. *Combustion and Flame*, 157(10):1879–1898, 2010. doi:10.1016/j.combustflame.2010.07.009.
- [54] R. Niranjana and A. K. Thakur. The toxicological mechanisms of environmental soot (black carbon) and carbon black: Focus on oxidative stress and inflammatory pathways. *Frontiers in Immunology*, 8:763, 2017. doi:10.3389/fimmu.2017.00763.
- [55] N. Peters and B. Rogg. *Reduced Kinetic Mechanisms for Applications in Combustion Systems*. Springer-Verlag Berlin Heidelberg, 1993. doi:10.1007/978-3-540-47543-9.
- [56] S. B. Pope. Small scales, many species and the manifold challenges of turbulent combustion. *Proceedings of the Combustion Institute*, 34(1):1–31, 2013. doi:10.1016/j.proci.2012.09.009.

- [57] J. Prager, H. N. Najm, M. Valorani, and D. A. Goussis. Skeletal mechanism generation with CSP and validation for premixed n-heptane flames. *Proceedings of the Combustion Institute*, 32 I(1):509–517, 2009. doi:10.1016/j.proci.2008.06.074.
- [58] A. Raj, M. Celnik, R. Shirley, M. Sander, R. Patterson, R. West, and M. Kraft. A statistical approach to develop a detailed soot growth model using PAH characteristics. *Combustion and Flame*, 156(4):896–913, 2009. doi:10.1016/j.combustflame.2009.01.005.
- [59] A. Raj, M. Sander, V. Janardhanan, and M. Kraft. A study on the coagulation of polycyclic aromatic hydrocarbon clusters to determine their collision efficiency. *Combustion and Flame*, 157(3):523–534, 2010. doi:10.1016/j.combustflame.2009.10.003.
- [60] A. Raj, I. D. C. Prada, A. A. Amer, and S. H. Chung. A reaction mechanism for gasoline surrogate fuels for large polycyclic aromatic hydrocarbons. *Combustion and Flame*, 159(2):500–515, 2012. doi:10.1016/j.combustflame.2011.08.011.
- [61] V. Ramanathan and G. Carmichael. Global and regional climate changes due to black carbon. *Nature Geoscience*, 1:221 – 227, 2008. doi:10.1038/ngeo156.
- [62] E. Ranzi and T. Faravelli. CRECK Modeling Group, 2015. Accessed 01 March 2019.
- [63] E. Ranzi, A. Frassoldati, R. Grana, A. Cuoci, T. Faravelli, A. P. Kelley, and C. K. Law. Hierarchical and comparative kinetic modeling of laminar flame speeds of hydrocarbon and oxygenated fuels. *Progress in Energy and Combustion Science*, 38(4):468–501, 2012. doi:10.1016/j.pecs.2012.03.004.
- [64] S. P. Roy and D. C. Haworth. A systematic comparison of detailed soot models and gas-phase chemical mechanisms in laminar premixed flames. *Combustion Science and Technology*, 188(7):1021–1053, 2016. doi:10.1080/00102202.2016.1145117.
- [65] M. Sander, R. I. A. Patterson, A. Braumann, A. Raj, and M. Kraft. Developing the PAH-PP soot particle model using process informatics and uncertainty propagation. *Proceedings of the Combustion Institute*, 33(1):675–683, 2011. doi:10.1016/j.proci.2010.06.156.
- [66] J. Singh, M. Balthasar, M. Kraft, and W. Wagner. Stochastic modeling of soot particle size and age distributions in laminar premixed flames. *Proceedings of the Combustion Institute*, 30(1):1457–1464, 2005. doi:10.1016/j.proci.2004.08.120.
- [67] R. Singh and M. Frenklach. A mechanistic study of the influence of graphene curvature on the rate of high-temperature oxidation by molecular oxygen. *Carbon*, 101:203–212, 2016. doi:10.1016/j.carbon.2016.01.090.
- [68] R. I. Singh, A. M. Mebel, and M. Frenklach. Oxidation of graphene-edge six- and five-member rings by molecular oxygen. *Journal of Physical Chemistry A*, 119(28):7528–7547, 2015. doi:10.1021/acs.jpca.5b00868.

- [69] N. A. Slavinskaya and P. Frank. A modelling study of aromatic soot precursors formation in laminar methane and ethene flames. *Combustion and Flame*, 156(9): 1705–1722, 2009. doi:10.1016/j.combustflame.2009.04.013.
- [70] N. A. Slavinskaya, U. Riedel, S. B. Dworkin, and M. J. Thomson. Detailed numerical modeling of PAH formation and growth in non-premixed ethylene and ethane flames. *Combustion and Flame*, 159(3):979–995, 2012. doi:10.1016/j.combustflame.2011.10.005.
- [71] A. Smallbone, A. Bhave, A. R. Coble, S. Mosbach, M. Kraft, and R. McDavid. *Identifying Optimal Operating Points in Terms of Engineering Constraints and Regulated Emissions in Modern Diesel Engines*. SAE International, 2011-01-1388. doi:10.4271/2011-01-1388.
- [72] M. D. Smooke, R. J. Hall, M. B. Colket, J. Fielding, M. B. Long, C. S. McEnally, and L. D. Pfefferle. Investigation of the transition from lightly sooting towards heavily sooting co-flow ethylene diffusion flames. *Combustion Theory and Modelling*, 8(3): 593–606, 2004. doi:10.1088/1364-7830/8/3/009.
- [73] S. E. Stein and A. Fahr. High-temperature stabilities of hydrocarbons. *The Journal of Physical Chemistry*, 89(17):3714–3725, 1985. doi:10.1021/j100263a027.
- [74] A. Tikhonov. Systems of differential equations containing small parameters for derivatives. *Mat. Sb.*, 31 (73)(3):575–586, 1952. In Russian.
- [75] T. Turányi and A. S. Tomlin. *Analysis of Kinetic Reaction Mechanisms*. Springer, Berlin, Heidelberg, 2015. doi:10.1007/978-3-662-44562-4.
- [76] T. Turányi, A. S. Tomlin, and M. J. Pilling. On the error of the quasi-steady-state approximation. *Journal of Physical Chemistry*, 97(1):163–172, 1993. doi:10.1021/j100103a028.
- [77] B. V. Unterreiner, M. Sierka, and R. Ahlrichs. Reaction pathways for growth of polycyclic aromatic hydrocarbons under combustion conditions, a DFT study. *Physical Chemistry Chemical Physics*, 6(18):4377–4384, 2004. doi:10.1039/b407279k.
- [78] A. Veshkini, S. B. Dworkin, and M. J. Thomson. A soot particle surface reactivity model applied to a wide range of laminar ethylene/air flames. *Combustion and Flame*, 161(12):3191–3200, 2015. doi:10.1016/j.combustflame.2014.05.024.
- [79] A. Violi, A. Kubota, T. Truong, W. Pitz, C. Westbrook, and A. Sarofim. A fully integrated kinetic Monte Carlo/molecular dynamics approach for the simulation of soot precursor growth. *Proceedings of the Combustion Institute*, 29(2):2343–2349, 2002. doi:10.1016/S1540-7489(02)80285-1.
- [80] H. Wang. Formation of nascent soot and other condensed-phase materials in flames. *Proceedings of the Combustion Institute*, 33(1):41–67, 2011. doi:10.1016/j.proci.2010.09.009.

- [81] H. Wang and M. Frenklach. A detailed kinetic modeling study of aromatics formation in laminar premixed acetylene and ethylene flames. *Combustion and Flame*, 110(1-2):173–221, 1997. doi:10.1016/S0010-2180(97)00068-0.
- [82] Y. Wang, A. Raj, and S. H. Chung. A PAH growth mechanism and synergistic effect on PAH formation in counterflow diffusion flames. *Combustion and Flame*, 160(9):1667–1676, 2013. doi:10.1016/j.combustflame.2013.03.013.
- [83] Y. Wang, A. Raj, and S. H. Chung. Soot modeling of counterflow diffusion flames of ethylene-based binary mixture fuels. *Combustion and Flame*, 162(3):586–596, 2015. doi:10.1016/j.combustflame.2014.08.016.
- [84] R. Whitesides and M. Frenklach. Detailed kinetic Monte Carlo simulations of graphene-edge growth. *The Journal of Physical Chemistry A*, 114(2):689–703, 2010. doi:10.1021/jp906541a.
- [85] R. Whitesides and M. Frenklach. Effect of reaction kinetics on graphene-edge morphology and composition. *Zeitschrift für Physikalische Chemie*, 229(4):597–614, 2015. doi:10.1515/zpch-2014-0633.
- [86] E. K. Yapp, C. G. Wells, J. Akroyd, S. Mosbach, R. Xu, and M. Kraft. Modelling PAH curvature in laminar premixed flames using a detailed population balance model. *Combustion and Flame*, 176:172–180, 2017. doi:10.1016/j.combustflame.2016.10.004.